NASA Technical Paper 1167

Flight Evaluation of the Transonic Stability and Control Characteristics of an Airplane Incorporating a Supercritical Wing

Neil W. Matheny and Donald H. Gatlin

FEBRUARY 1978

NASA

NASA Technical Paper 1167

Flight Evaluation of the Transonic Stability and Control Characteristics of an Airplane Incorporating a Supercritical Wing

Neil W. Matheny and Donald H. Gatlin
Dryden Flight Research Center
Edwards, California

National Aeronautics
and Space Administration

Scientific and Technical
Information Office

1978

FLIGHT EVALUATION OF THE TRANSONIC STABILITY AND CONTROL CHARACTERISTICS OF AN AIRPLANE INCORPORATING A SUPERCRITICAL WING

Neil W. Matheny and Donald H. Gatlin
Dryden Flight Research Center

INTRODUCTION

The supercritical airfoil conceived by Richard T. Whitcomb at the NASA Langley Research Center has been shown to be an improvement on conventional airfoils, particularly at transonic Mach numbers. Early wind tunnel tests showed that wings incorporating supercritical airfoils could be developed that allowed improvements over conventional wings by increasing the wing's thickness-to-chord ratio without decreasing the drag rise Mach number, or by improving aircraft maneuver performance at advanced load factors without complex maneuver devices, or by raising the aircraft drag rise Mach number. These performance benefits are being investigated in three full-scale flight test programs. The results of flight tests made with a T-2C aircraft with an unswept supercritical wing to investigate the effects of the increased wing thickness-to-chord ratio are reported in references 1 and 2. Flight tests are currently being made at the NASA Dryden Flight Research Center (DFRC) to investigate the effects of a supercritical airfoil on the maneuver performance of an aircraft with a variable sweep wing; these tests utilize an F-111A airplane as a test bed. The third performance benefit—increased drag rise Mach number—was investigated in a flight test program at DFRC using a modified TF-8A aircraft. This report discusses the stability and control characteristics of that airplane.

The TF-8A aircraft was fitted with a swept, high aspect ratio supercritical wing. The vehicle was designed for a transport mission at a cruise Mach number of 0.99. Basic TF-8A structures and systems were retained to the maximum extent possible. No unusual effort was made to optimize stability augmentation systems or aircraft aerodynamic characteristics for handling qualities. Preliminary results of this program are reported in reference 3, and final results are reported in references 4 to 6.

This report describes the stability and control characteristics of the test vehicle, with emphasis on flight at transonic Mach numbers. It compares flight-determined

derivatives with rigid model wind tunnel predictions and discusses some aspects of the vehicle's handling qualities. The test pilot's impressions of the vehicle's handling qualities are described at length in reference 3.

SYMBOLS AND ABBREVIATIONS

Data are presented in terms of standard NASA coefficients of forces and moments, which are referenced to axes passing through the center of gravity. The positive directions are: X, forward; Y, to the right; Z, down. Positive directions of the forces, moments, and angular displacements and velocities are in accord with the right-hand rule.

Physical quantities in this report were measured in the International System of Units (SI).

A	matrix of stability coefficients
$APRA$	matrix of *a priori* weighting factors for the A matrix
$APRB$	matrix of *a priori* weighting factors for the B matrix
a_n	normal acceleration, g
a_y	transverse acceleration, g
B	matrix of control coefficients
b	wingspan, m
C_L	lift coefficient, $\frac{\text{Lift force}}{\bar{q}S}$
C_{L_q}	$= \frac{\partial C_L}{\partial \frac{q\bar{c}}{2V}}$, per rad
C_{L_α}	$= \frac{\partial C_L}{\partial \alpha}$, per deg
$C_{L_{\delta_e}}$	$= \frac{\partial C_L}{\partial \delta_e}$, per deg

C_l rolling-moment coefficient, $\frac{\text{Rolling moment}}{\bar{q}Sb}$

C_{l_p} $= \frac{\partial C_l}{\partial \frac{pb}{2V}}$, per rad

C_{l_r} $= \frac{\partial C_l}{\partial \frac{rb}{2V}}$, per rad

C_{l_β} $= \frac{\partial C_l}{\partial \beta}$, per deg

$C_{l_{\dot{\beta}}}$ $= \frac{\partial C_l}{\partial \frac{\dot{\beta}b}{2V}}$, per rad

$C_{l_{\delta_a}}$ $= \frac{\partial C_l}{\partial \delta_a}$, per deg

$C_{l_{\delta_r}}$ $= \frac{\partial C_l}{\partial \delta_r}$, per deg

C_m pitching-moment coefficient, $\frac{\text{Pitching moment}}{\bar{q}S\bar{c}}$

C_{m_0} pitching-moment coefficient at zero lift

C_{m_q} $= \frac{\partial C_m}{\partial \frac{q\bar{c}}{2V}}$, per rad

C_{m_α} $= \frac{\partial C_m}{\partial \alpha}$, per deg

$C_{m_{\dot{\alpha}}}$ $= \frac{\partial C_m}{\partial \frac{\dot{\alpha}\bar{c}}{2V}}$, per deg

$C_{m_{\delta_e}}$ $= \dfrac{\partial C_m}{\partial \delta_e}$, per deg

C_N normal force coefficient, $\dfrac{\text{Normal force}}{\bar{q}S}$

C_n yawing-moment coefficient, $\dfrac{\text{Yawing moment}}{\bar{q}Sb}$

C_{n_p} $= \dfrac{\partial C_n}{\partial \frac{pb}{2V}}$, per rad

C_{n_r} $= \dfrac{\partial C_n}{\partial \frac{rb}{2V}}$, per rad

C_{n_β} $= \dfrac{\partial C_n}{\partial \beta}$, per deg

$C_{n_{\dot{\beta}}}$ $= \dfrac{\partial C_n}{\partial \frac{\dot{\beta}b}{2V}}$, per rad

$C_{n_{\delta_a}}$ $= \dfrac{\partial C_n}{\partial \delta_a}$, per deg

$C_{n_{\delta_r}}$ $= \dfrac{\partial C_n}{\partial \delta_r}$, per deg

C_y side force coefficient, $\dfrac{\text{Side force}}{\bar{q}S}$

C_{y_p} $= \dfrac{\partial C_y}{\partial \frac{pb}{2V}}$, per rad

C_{y_r} $= \dfrac{\partial C_y}{\partial \frac{rb}{2V}}$, per rad

C_{y_β} $= \frac{\partial C_y}{\partial \beta}$, per deg

$C_{y_{\delta_a}}$ $= \frac{\partial C_y}{\partial \delta_a}$, per deg

$C_{y_{\delta_r}}$ $= \frac{\partial C_y}{\partial \delta_r}$, per deg

$\bar{c}$ mean aerodynamic chord, m

$D1$ matrix of state variable weighting factors

h_p geopotential altitude, m

I_X, I_Y, I_Z moments of inertia about body X-, Y-, and Z-axes, respectively, kg/m^2

I_{XZ} moment of inertia about body XZ plane, kg/m^2

L rolling-moment coefficient, $\frac{\text{Rolling moment}}{I_X}$, per sec^2

L_{δ_a} $= \frac{\partial L}{\partial \delta_a}$, per sec^2/rad

M Mach number

MMLE maximum likelihood estimation

n normal load factor, g

p, q, r time rate of change of roll, pitch, and yaw about body X-, Y-, and Z-axes, respectively, rad/sec (unless noted otherwise)

$\bar{q}$ dynamic pressure, N/m^2

S wing area, m^2

t time, sec

V velocity, m/sec

α	angle of attack, deg
β	angle of sideslip, deg
γ	flightpath angle, deg
δ_a	aileron deflection, deg
δ_e	stabilizer deflection, deg
δ_r	rudder deflection, deg
θ, φ	Euler angles of pitch and roll, respectively, deg
τ_R	roll mode time constant, sec
ω_d	natural frequency of denominator of φ/δ_a transfer function, rad/sec
$\omega_{n_{sp}}$	longitudinal short period natural frequency, rad/sec
ω_φ	natural frequency of numerator of φ/δ_a transfer function, rad/sec

Subscripts:

cg	measured at center of gravity
max	maximum

A dot over a parameter indicates the time derivative of the associated quantity.

AIRPLANE DESCRIPTION

The TF-8A airplane was modified by incorporating a fixed incidence high aspect ratio supercritical wing (fig. 1). The configuration was intended to be representative of transonic cruise transports and was designed for flight at a lift coefficient of 0.4 and a Mach number of 0.99. A major design constraint was to make the fewest modifications possible to the aircraft to minimize the effects of the fuselage on the wing's performance. Fairings were added at the forward wing-fuselage junctures and along the upper fuselage between the wing and vertical fin to improve the cross-sectional area distribution. The vertical and horizontal stabilizers of the basic TF-8A aircraft were not changed. A vortex generator (fig. 2) was installed on the leading edge of each wing at the 60-percent semispan station to alleviate an unstable break in pitching moment at moderate lift coefficients. The test vehicle's physical characteristics are listed in table 1. Additional information

on the aircraft design philosophy and dimensional details are contained in references 3, 7, 8, and 9.

CONTROL SYSTEM

The airplane was equipped with a mechanically controlled, hydraulically actuated, irreversible control system that was essentially the same as in the basic TF-8A airplane. The aerodynamic controls consisted of the rudder, an all-movable horizontal stabilizer, and midspan ailerons. The ailerons were drooped 20° for takeoff and landing and were sized for landing in 15-knot crosswinds. No other high-lift devices were used.

STABILITY AUGMENTATION SYSTEMS

The roll and yaw stability augmentation systems were essentially the same as in the basic TF-8A airplane in the cruise condition. However, the automatic gain schedule was replaced with manual gain controls that were adjustable in the cockpit. In addition, a full-time aileron-to-rudder interconnect with manual gain control was incorporated.

An all-new command augmentation system incorporating blended pitch rate and normal acceleration feedback was used in the pitch axis. This system augmented pitch damping and provided nearly constant longitudinal sensitivity and stick force gradients throughout the flight envelope. An autotrim (servo centering) function was also provided. The bobweight of the basic TF-8A pitch feel system was retained.

Block diagrams of the stability augmentation systems are shown in figure 3.

WEIGHT, BALANCE, AND INERTIAS

Airplane gross weight and center of gravity position were computed from static weight and balance measurements and from contractor-supplied data on internal fuel distribution. The standard airplane fuel-quantity measurement system was instrumented to provide continuous readouts. Aircraft inertias were determined about the airplane reference axes from contractor-supplied data on the unmodified airplane and the new wing installation. Adjustments were made for ballast, avionics, and instrumentation. The inertias were estimated to be accurate within 10 percent.

FLIGHT TEST CONDITIONS AND DATA ANALYSIS

All flight tests were performed in the vicinity of Edwards Air Force Base, Edwards, Calif. Test Mach numbers ranged from 0.29 to 1.20, and altitude ranged from 2,900 meters to 15,400 meters. Aircraft gross weight ranged from 97.3 kilonewtons to 108.4 kilonewtons, and angle of attack ranged from 1.6° to 14.0°. The position of the center of gravity ranged between 20 percent $\bar{c}$ and 25 percent $\bar{c}$. Most of the evaluation maneuvers performed consisted of control pulses and doublets and slowly increasing quasi-steady windup turns. The control pulses and doublets were performed in each axis with the stability augmentation system for that axis off. Thrust was adjusted as necessary to maintain constant Mach number; thrust effects were ignored. Other types of maneuvers were performed to investigate specific characteristics and handling qualities. Pilot comments were obtained from both operational and evaluation maneuvers.

The flight test aerodynamic derivatives contained herein were determined by using a version of the modified maximum likelihood estimation (MMLE) program described in reference 10. The *a priori* values of the input matrices (A and B) were obtained from rigid model wind tunnel tests. The *a priori* weighting matrices, $APRA$ and $APRB$, and the signal weighting matrix, $D1$, were determined early in the analysis and remained constant thereafter. Table 2 lists the values used in the $APRA$, $APRB$, and $D1$ matrices for both the longitudinal and lateral-directional derivatives. Each run that was used for derivative determination was reviewed for maneuver quality, the possibility of extraneous inputs, quality of time history match, and the resulting weighted error sum before the derivatives were accepted as final. All derivatives were corrected to a center of gravity position of 25 percent $\bar{c}$ unless otherwise stated. The longitudinal derivatives are referenced to the stability axis system, and the lateral-directional derivatives are referenced to the body axis system.

The pitching-moment data presented as a function of normal force coefficient were obtained from windup turn maneuvers. These data were corrected to a fixed elevator control position by using the flight-determined values of elevator control effectiveness, $C_{L_{\delta_e}}$ and $C_{m_{\delta_e}}$, and the pitch damping derivative, $C_{m_q} + C_{m_{\dot{\alpha}}}$. Airplane dynamic characteristics, such as $\omega_{n_{sp}}$, were computed from the flight-determined derivatives.

WIND TUNNEL TESTS

All wind tunnel tests for this program were conducted at the NASA Langley Research Center in the 8-Foot Transonic Pressure Tunnel and the 16-Foot Transonic Tunnel. The tunnels and test apparatus are described in references 11 and 12, respectively. The data acquired included static force data (ref. 7), pressure distribution data (ref. 8), aerodynamic loads data (ref. 11), aileron control data (ref. 13), and dynamic force data (ref. 14).

The tests were performed on a 0.087-scale model using two test wings, one of steel and one of aluminum. Most of the force and moment data used for performance estimates and all of the pressure measurements were obtained from tests using the steel wing. The aluminum wing was used to predict aileron and flap effectiveness. For these tests, the tunnel's dynamic pressures were reduced in an effort to obtain aeroelastic deflections for the aluminum wing that were comparable to those for the steel wing. The predicted aerodynamic derivatives presented herein were determined from tests made with the steel wing, when such data were available; the data were considered to be for a rigid model. All wind tunnel data are referenced to a center of gravity position of 25 percent $\bar{c}$.

The aileron control derivatives were determined for aileron deflections of ±5°, and the sideslip derivatives were determined for sideslip angles of ±2°. The wind tunnel test Mach numbers ranged from 0.25 to 1.20, and Reynolds number ranged from 2×10^6 to 4×10^6 based on a model mean aerodynamic chord of 0.181 meter.

The full-scale wing was constructed to duplicate the aerodynamic shape of the steel wing model at the design lift coefficient of 0.4 at Mach 0.99.

RESULTS AND DISCUSSION

Longitudinal Derivatives

Longitudinal derivatives were determined primarily from elevator pulses and occasionally from slower pushover or pullup maneuvers. Typical time histories comparing the response computed from MMLE with the flight data for both maneuver types are shown in figure 4. All the longitudinal data in this report are the result of similar matches.

Variations of the longitudinal derivatives C_{m_α}, $C_{m_{\delta_e}}$, C_{L_α}, $C_{L_{\delta_e}}$, and $C_{m_q} + C_{m_{\dot{\alpha}}}$ with angle of attack are presented in figure 5 for Mach numbers of 0.50, 0.80, 0.90, 0.95, 0.97, 0.99, 1.02, and 1.20. Faired rigid wind tunnel data are presented for comparison. The derivative C_{L_q} is not presented because there was insufficient information in the data for its determination. Angle of attack ranged from 1.7° to 6.2°.

Flight data acquired over a small range of Mach numbers are presented together. This contributes to an appearance of scatter in the flight data in comparison with the faired wind tunnel data. In general, the trend of the flight data follows the predictions. The longitudinal stability derivative, C_{m_α}, shows slightly higher stability (is more negative) over the Mach number range tested. The pitch damping parameter, $C_{m_q} + C_{m_{\dot{\alpha}}}$, indicates damping to be lower than predicted throughout

the subsonic range. A summary of the data for an angle of attack of 3° (near the design lift coefficient) is presented as a function of Mach number in figure 6.

The higher level of airplane stability in flight is believed to be due, in part, to higher velocity peaks near the trailing edge of the wing than obtained in the wind tunnel and to a more rearwards location of the shock at supercritical speeds (ref. 4).

Lateral-Directional Derivatives

The lateral-directional derivatives were determined from either aileron or rudder pulses by using the MMLE program. Typical time history comparisons for each maneuver type are shown in figure 7.

The derivatives were determined over a Mach number range from 0.75 to 1.01 and an angle of attack range from 1.6° to 7.9°. Variations in the derivatives with angle of attack are presented in figure 8 for Mach numbers of 0.80, 0.90, 0.95, and 0.99. Faired rigid wind tunnel data are presented for comparison. The derivatives $C_{y_{\delta_a}}$ and C_{l_r} are not presented because there was insufficient information in the data for their determination. Flight data ranging in Mach number from 0.75 to 0.85 are presented as Mach 0.80 data. Similarly, Mach 0.90 data range from Mach 0.85 to Mach 0.93, Mach 0.95 data range from Mach 0.93 to Mach 0.97, and Mach 0.99 data range from Mach 0.97 to Mach 1.01.

In general, the flight data follow the wind tunnel trends at the lower Mach numbers, with discrepancies becoming more significant transonically. The sideslip derivatives C_{l_β} and C_{n_β} (figs. 8(a) and 8(b)) show fair agreement at Mach numbers of 0.80 and 0.90 but differ by 30 percent to 40 percent at Mach 0.95 and Mach 0.99. The values of C_{l_β} show a strong effect of angle of attack transonically, with the maximum difference between the flight and wind tunnel data occurring at Mach 0.99 and an angle of attack of 4°. The derivative C_{n_β} is consistently lower than predicted, but shows trends with angle of attack similar to the predicted values. The rudder derivatives $C_{n_{\delta_r}}$ and $C_{y_{\delta_r}}$ (figs. 8(e) and 8(f)) show similar Mach number trends but exhibit the greatest discrepancy at an angle of attack of 2° and are in good agreement at 4°. The flight values of aileron roll control power, $C_{l_{\delta_a}}$ (fig. 8(g)), are consistently larger than the wind tunnel values at the lower Mach numbers, with the differences diminishing as the design point is approached. This difference is believed to be caused primarily by the higher than expected velocity peaks near the wing trailing edge, as mentioned previously.

The scatter in the flight data for $C_{l_{\delta_a}}$ is believed to be due primarily to the nonlinear character of this derivative as a function of control position. Aileron inputs were typically between ±5° and ±10° in flight, whereas the predictions are based on deflections of ±5°.

The lateral-directional derivatives are summarized as functions of Mach number in figure 9 for an angle of attack of 3°. This figure shows that the absolute values of C_{l_β} and $C_{l_{\delta_a}}$ (figs. 9(a) and 9(g)) from the flight tests are greater than predicted; that the absolute values of C_{n_β}, C_{y_β}, $C_{n_{\delta_r}}$, and $C_{y_{\delta_r}}$ (figs. 9(b), 9(c), 9(e), and 9(f)) from flight tests are less than predicted; and that the flight and predicted values of the other derivatives are in generally good agreement.

Longitudinal Stability and Control

Vehicle response to longitudinal control inputs was evaluated in part by referring to the current military flying qualities specification (ref. 15). For acceptable handling qualities, this specification requires the combinations of short period frequency and normal acceleration per radian of angle of attack shown in figure 10 for transport aircraft at cruise flight conditions. The level 1 boundaries are for flight with all systems functioning. Levels 2 and 3 indicate acceptable values for flight with system failures that increase the pilot's workload; at level 3, the failures lead to mission termination. The flight data represent the unaugmented airplane for the transonic range (Mach 0.80 to Mach 1.20) and are about midway between the level 1 bounds, indicating generally satisfactory response. The flight data are in good agreement with predictions. The pilots considered both the augmented and unaugmented airplane's longitudinal response to be satisfactory.

The specification also identifies minimum short period damping levels. The augmented airplane met these criteria; however, both the predicted and flight-measured damping ratios for the unaugmented vehicle were approximately 30 percent below the level 1 requirements. The unaugmented vehicle was lightly damped and tended to overshoot.

Trim variations during transonic acceleration are also of interest to the transport pilot. Other aircraft have exhibited airplane noseup trim requirements at high subsonic Mach numbers that required compensation in one form or another. An airplane noseup trim requirement of approximately 1° was predicted for the test airplane between Mach 0.99 and Mach 1.02. However, this variation did not appear in flight. Figure 11 shows the variation of stabilizer angle for trim with Mach number for a level acceleration-deceleration maneuver performed at an altitude of 13,700 meters. Speed stability was nearly neutral between Mach 0.90 and Mach 1.05. Stick-force variation is not shown because the pitch augmentation system provided apparent neutral speed stability for all conditions.

Below Mach 1.00, the stabilizer angle required for trim is approximately 1° more trailing edge up than was predicted from model tests. Part of this discrepancy can be attributed to the higher than predicted trend of the flight values for C_{m_α} (fig. 5). In addition, some of the discrepancy is believed to be due to differences between flight and predicted values of zero lift pitching moment, C_{m_0}. Figure 12 compares the flight values for C_{m_0} with those predicted from wind tunnel measurements. The flight values were estimated from measurements of aerodynamic center location and stabilizer effectiveness. Below Mach 0.95, there is a considerable difference between the flight and predicted values, with the flight data showing a larger nosedown moment. Contributing to this difference is the more negative than predicted pressure measured along the wing trailing edge (ref. 4).

The maneuverability of the test airplane was satisfactory in the transonic range, particularly at design cruise conditions. The vehicle exhibited a mild pitchup. Pitchup was predicted from wind tunnel data as the point where $\frac{\Delta C_m}{\Delta C_L}$ equaled zero for a center of gravity position of 25 percent $\bar{c}$ and is shown as a function of C_N in figure 13. The flight values in figure 13 were determined from plots of stabilizer angle versus angle of attack and are in general agreement with the predictions. The flight data are also for center of gravity positions near 25 percent $\bar{c}$. Pilot comments indicate that the pitchup was completely masked by the augmentation system and that the augmented airplane was readily controllable. The sharp rise in the pitchup boundary above Mach 0.90 is attributed to a rearward shift of the wing shock wave to the vicinity of the trailing edge. This shock is stabilized in the rear location and prevents the flow separation from spreading forward. This in turn prevents large lift losses from occurring on the outboard wing sections until high angles of attack are reached. The flight-determined buffet onset boundary (ref. 6) shows where flow separation begins.

A comparison of flight and predicted normal force and pitching-moment characteristics for a fixed stabilizer position at a Mach number of 0.95 is shown in figure 14. The flight results were obtained by correcting data obtained during a slow windup turn to the stabilizer setting of the predicted data by using flight values of $C_{m_{\delta_e}}$. The data were chosen in such a way as to minimize the effects of pitch rate and pitch acceleration. The trends of the flight and wind tunnel results are similar. The normal-force curves agree particularly well. As noted in figure 5, however, the pitching moments from flight show slightly higher stability (more negative values) than predicted. A reduction in stability is indicated in the flight data at an angle of attack of approximately 7°. This is followed by an abrupt pitchup at an angle of attack of approximately 11°. The wind tunnel data also show the noseup tendency at an angle of attack of approximately 7° and an abrupt pitchup near an angle of attack of 13°. Buffet onset is generally observed in flight at the first break in the pitch curve.

The effects of the vortex generators on the airplane's longitudinal static stability are apparent in figure 15, where the flight data in figure 14 are compared with the data from a similar windup turn with the vortex generators off. The figure shows that the vortex generators delayed flow separation and the associated reduction in static stability to a higher normal force coefficient and significantly reduced the severity of the pitchup. At the angles of attack below flow separation, static stability was the same.

These variations in the stability of the aircraft with the vortex generators both on and off are masked by the pitch command augmentation system.

Lateral-Directional Stability and Control

The airplane's Dutch roll characteristics were satisfactory under all flight conditions except at high angles of attack in the transonic range (Mach 0.80 to Mach 1.00) with the roll and yaw stability augmentation systems off. The low Dutch roll damping and roll control power were rated unsatisfactory under these circumstances.

Good roll response requires a minimum of coupling between the roll and yaw axes. Flight and predicted values of the unaugmented airplane's roll response near cruise angles of attack are compared with the criteria described in reference 16 in figure 16. When ω_φ equals ω_d, pure roll response is obtained. When ω_φ is greater than ω_d, there is a tendency for pilot-induced oscillations, and when ω_φ is less than ω_d, response is sluggish. The flight and predicted data at cruise conditions are in good agreement and lie primarily in an area considered to be satisfactory.

At higher angles of attack than shown in figure 16, the unaugmented airplane's roll characteristics were generally unsatisfactory because of the combined high adverse yaw and effective dihedral. This resulted in a slow response to lateral control inputs that became unacceptable near the limit angles of attack.

The maximum roll control capability of the test vehicle at cruise angles of attack is shown in figure 17 as a function of roll mode time constant. The boundaries are for transport aircraft and were determined from flight tests of the Dryden Flight Research Center variable-stability JetStar airplane (ref. 17). The flight data for the unaugmented supercritical wing airplane are near the predictions made for the Mach number range shown, even though in each case the flight value of $L_{\delta_a}\delta_{a_{max}}$ was higher than predicted. Both the flight and the predicted values of roll control power are greater than the indicated satisfactory range for transport aircraft, although the higher roll control power did not preclude flight testing.

A limited evaluation of the airplane's static directional stability was made from slowly increasing wings-level sideslips. Both rudder deflection, δ_r, and aileron deflection, δ_a, were found to be linear with increasing angle of sideslip to the

maximum angle of sideslip tested (4°). Results in terms of δ_r/β and δ_a/β versus Mach number are presented in figure 18. No corrections were made for differences in center of gravity position. In the cruise configuration, apparent directional stability, δ_r/β, increases from approximately 0.7 degree per degree at low Mach numbers to approximately 0.95 degree per degree at Mach 0.90. Apparent effective dihedral, δ_a/β, remains approximately constant with Mach number at approximately 1.7 degrees per degree. In the takeoff and landing configuration, the increased adverse yaw and effective dihedral of the drooped ailerons reduced δ_r/β to approximately 0.3 degree per degree and increased δ_a/β to 4.2 degrees per degree.

Upset and Overspeed Behavior

Another matter of concern to the transport pilot is the controllability of the aircraft in an upset or overspeed condition. Therefore, several upset maneuvers were performed with the test vehicle, starting from both wings-level flight and from banked attitudes near the design cruise speed. A time history of the most severe maneuver, which began with the aircraft banked approximately 45°, is shown in figure 19. An upset was initiated by pushing the aircraft over into a nearly 0g dive, holding for approximately 5 seconds with the throttle fixed, and then recovering with a 1.5g to 2.0g pullup.

The same overspeed maneuver is shown again in figure 20, which also shows the altitude and Mach number excursions resulting from two other upset maneuvers that were initiated from wings-level flight. All three maneuvers were performed with the stability augmentation system on. The two maneuvers that were started from level flight began at a Mach number of approximately 0.97, one from an altitude of approximately 14,000 meters, the other from an altitude of 15,000 meters. In the maneuver that was started at 15,000 meters, the airplane was held at 0.5g for 10 seconds before recovery was initiated; in the other maneuvers, the airplane was held for only 5 seconds. Because of the rapid rise in drag beyond the cruise Mach number, neither of the excursions from level flight extended much beyond Mach 1.00. The banked maneuver was performed in such a way that it exceeded Mach 1.00, but the aircraft was no more difficult to control during the maneuver.

Recovery from each maneuver was easy, and aircraft response was normal in all respects. Control power was adequate, and there was no tendency for wing drop or control reversal. The airplane was accelerated to supersonic speeds many times and handled nicely on each occasion.

CONCLUDING REMARKS

A flight test program was performed utilizing a TF-8A airplane equipped with a transport-type supercritical wing designed for cruise at Mach 0.99. Fuselage fairings were added to achieve the best possible area distribution within the

constraints of the program. A stability and control analysis of the airplane in transonic cruise flight and comparisons of flight and rigid model wind tunnel data had the following results:

The airplane's longitudinal static stability, C_{m_α}, was greater than predicted. This was thought to be due in part to velocity peaks near the trailing edge of the full-scale wing that were higher than predicted. The pitch damping derivative, $C_{m_q} + C_{m_{\dot{\alpha}}}$, showed damping to be lower than predicted.

The flight-measured dihedral effect, C_{l_β}, was generally higher than predicted, with the maximum difference appearing near an angle of attack of 4°. The static directional stability, C_{n_β}, was lower across both the Mach number and angle of attack ranges investigated. Roll control power, $C_{l_{\delta_a}}$, was higher than predicted at the lower Mach numbers, but agreement improved as Mach number increased toward the design point.

The test vehicle exhibited acceptable handling qualities over the flight envelope with the stability augmentation system on. In terms of lateral-directional characteristics, the unaugmented airplane had low Dutch roll damping, low roll control power at high angles of attack, and roll control power at a greater than satisfactory level for a transport aircraft in cruising flight. Longitudinally, the aircraft exhibited a mild pitchup tendency. Leading edge vortex generators delayed the onset of flow separation, moving the pitchup point to a higher lift coefficient and reducing its severity. The pitchup tendency, both with and without vortex generators, was adequately masked by the stability augmentation system.

No adverse handling qualities were observed during recovery from simulated upset and overspeed maneuvers from the design cruise speed using normal piloting techniques.

Dryden Flight Research Center
National Aeronautics and Space Administration
Edwards, Calif., March 10, 1977

REFERENCES

1. Palmer, W. E.; Elliott, D. W.; and White, J. E.: Flight and Wind Tunnel Evaluation of a 17% Thick Supercritical Airfoil on a T-2C Airplane. Vol. I—Basic Report. NR71H-150, North American Rockwell, July 31, 1971.

2. Elliott, D. W.: Flying Qualities Evaluations of a 17% Thick Supercritical Wing on a T-2C Airplane. NR71H-331, North American Rockwell, July 1971.

3. Supercritical Wing Technology—A Progress Report on Flight Evaluations. NASA SP-301, 1972.

4. Montoya, Lawrence C.; and Banner, Richard D.: F-8 Supercritical Wing Flight Pressure, Boundary-Layer, and Wake Measurements and Comparisons With Wind Tunnel Data. NASA TM X-3544, 1977.

5. Pyle, Jon S.; and Steers, Louis L.: Flight-Determined Lift and Drag Characteristics of an F-8 Airplane Modified With a Supercritical Wing With Comparisons to Wind-Tunnel Results. NASA TM X-3250, 1975.

6. DeAngelis, V. M.: Wing Panel Loads and Aileron Hinge Moments Measured in Flight on the F-8 Supercritical Wing Airplane Including Correlations With Wind Tunnel Data. NASA TM X-3098, 1974.

7. Bartlett, Dennis W.; and Harris, Charles D.: Aerodynamic Characteristics of an NASA Supercritical-Wing Research Airplane Model With and Without Fuselage Area-Rule Additions at Mach 0.25 to 1.00. NASA TM X-2633, 1972.

8. Harris, Charles D.; and Bartlett, Dennis W.: Tabulated Pressure Measurements on an NASA Supercritical-Wing Research Airplane Model With and Without Fuselage Area-Rule Additions at Mach 0.25 to 1.00. NASA TM X-2634, 1972.

9. Harris, Charles D.; and Bartlett, Dennis W.: Wind-Tunnel Investigation of Effects of Underwing Leading-Edge Vortex Generators on a Supercritical-Wing Research Airplane Configuration. NASA TM X-2471, 1972.

10. Maine, Richard E.; and Iliff, Kenneth W.: A FORTRAN Program for Determining Aircraft Stability and Control Derivatives From Flight Data. NASA TN D-7831, 1975.

11. Harris, Charles D.: Wind-Tunnel Measurements of Aerodynamic Load Distribution on an NASA Supercritical-Wing Research Airplane Configuration. NASA TM X-2469, 1972.

12. Re, Richard J.: Stability and Control Characteristics, Including Aileron Hinge Moments, of a Model of a Supercritical-Wing Research Airplane. NASA TM X-2929, 1974.

13. Bartlett, Dennis W.: Effects of Differential and Symmetrical Aileron Deflection on the Aerodynamic Characteristics of an NASA Supercritical-Wing Research Airplane Model. NASA TM X-3231, 1975.

14. Boyden, Richmond P.: Dynamic Stability Characteristics in Pitch, Yaw, and Roll of a Supercritical-Wing Research Airplane Model. NASA TM X-2900, 1974.

15. Flying Qualities of Piloted Airplanes. Military Specification MIL-F-8785B(ASG), Aug. 7, 1969.

16. Taylor, Lawrence W., Jr.; and Iliff, Kenneth W.: Fixed-Base Simulator Pilot Rating Surveys for Predicting Lateral-Directional Handling Qualities and Pilot Rating Variability. NASA TN D-5358, 1969.

17. Holleman, Euclid C.: Flight Investigation of the Roll Requirements for Transport Airplanes in Cruising Flight. NASA TN D-5957, 1970.

TABLE 1.—PHYSICAL CHARACTERISTICS OF F-8 SUPERCRITICAL WING VEHICLE

Wing —	
Airfoil type	Supercritical
Area, m^2	25.506
Span, m	13.143
Mean aerodynamic chord, m	2.080
Root chord, m	2.84
Tip chord, m	1.04
Aspect ratio	6.77
Taper ratio	0.366
Thickness-to-chord ratio, percent:	
Root	11
Tip	7
Dihedral angle, deg	0
Quarter-chord sweep, deg	42.24
Incidence (root), deg	1.5
Twist, deg	-5
Aileron —	
Area, m^2	1.15
Span, m	2.36
Chord, percent wing chord	25
Deflection, deg	±15
Maximum droop (flap), deg	20
Horizontal stabilizer —	
Area, m^2	8.68
Span, m	5.52
Mean aerodynamic chord, m	1.86
Aspect ratio	3.51
Dihedral angle, deg	5.54
Quarter-chord sweep, deg	45
Vertical stabilizer —	
Area, m^2	10.13
Span, m	3.89
Mean aerodynamic chord, m	2.92
Aspect ratio	1.49
Quarter-chord sweep, deg	45

TABLE 1.—Concluded

Vortex generator —	
Location, percent semispan	60
Airfoil type	Clark Y
Span, m	0.15
Root chord, m	0.21
Thickness-to-chord ratio, percent	10
Leading edge sweep, deg	48
Mass characteristics —	
Zero fuel weight, kN	93.6
Maximum weight, kN	113.7
Center of gravity range, percent $\bar{c}$	20 to 25
I_X (typical), kg-m^2	20,555
I_Y (typical), kg-m^2	133,800
I_Z (typical), kg-m^2	147,850
I_{XZ} (typical), kg-m^2	4,185

TABLE 2.—VALUES USED IN *A PRIORI* AND SIGNAL WEIGHTING MATRICES

APRA weighting matrix —

Longitudinal:

C_{m_α}	5.0×10
C_{L_α}	3.0×10^3
$C_{m_q} + C_{m_{\dot{\alpha}}}$	2.5×10^3

Lateral-directional:

C_{y_β}	3.5×10^4
C_{l_β}	3.0×10^{-2}
C_{n_β}	3.0×10
C_{y_p}	3.0×10^5
$C_{l_p} + C_{l_{\dot{\beta}}} \sin \alpha$	1.0×10^3
$C_{n_p} + C_{n_{\dot{\beta}}} \sin \alpha$	1.6×10^4
C_{y_r}	0
C_{l_r}	1.0×10^4
$C_{n_r} - C_{n_{\dot{\beta}}} \cos \alpha$	1.6×10^3

APRB weighting matrix —

Longitudinal:

$C_{m_{\delta_e}}$	5.0×10
$C_{L_{\delta_e}}$	3.0×10^3

Lateral-directional:

$C_{y_{\delta_a}}$	3.5×10^7
$C_{l_{\delta_a}}$	3.0×10^{-3}
$C_{n_{\delta_a}}$	3.0×10^2

TABLE 2.—Concluded

$C_{y_{\delta_r}}$	3.5×10^3
$C_{l_{\delta_r}}$	3.0×10
$C_{n_{\delta_r}}$	3.0×10

$D1$ weighting matrix —

Longitudinal:

α	6.66×10^5
q	1.29×10^5
θ	2.56×10^5
$\dot{q}$	4.0×10^3
a_n	8.9×10^3

Lateral-directional:

β	2.0×10^6
p	1.15×10^4
r	2.8×10^5
φ	9.75×10^3
a_y	2.0×10^4

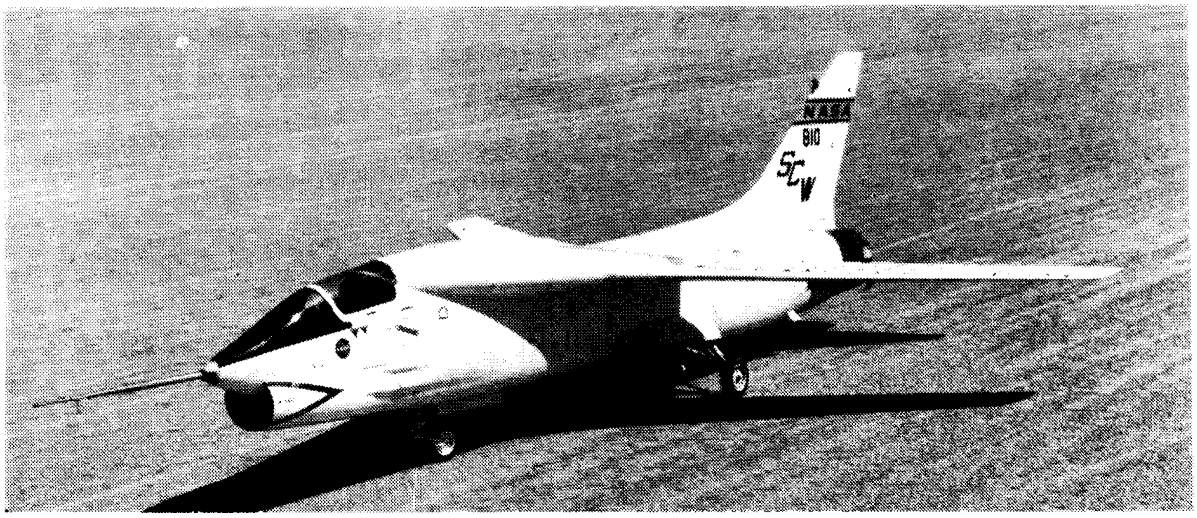

E-23122

(a) Three-quarter front view.

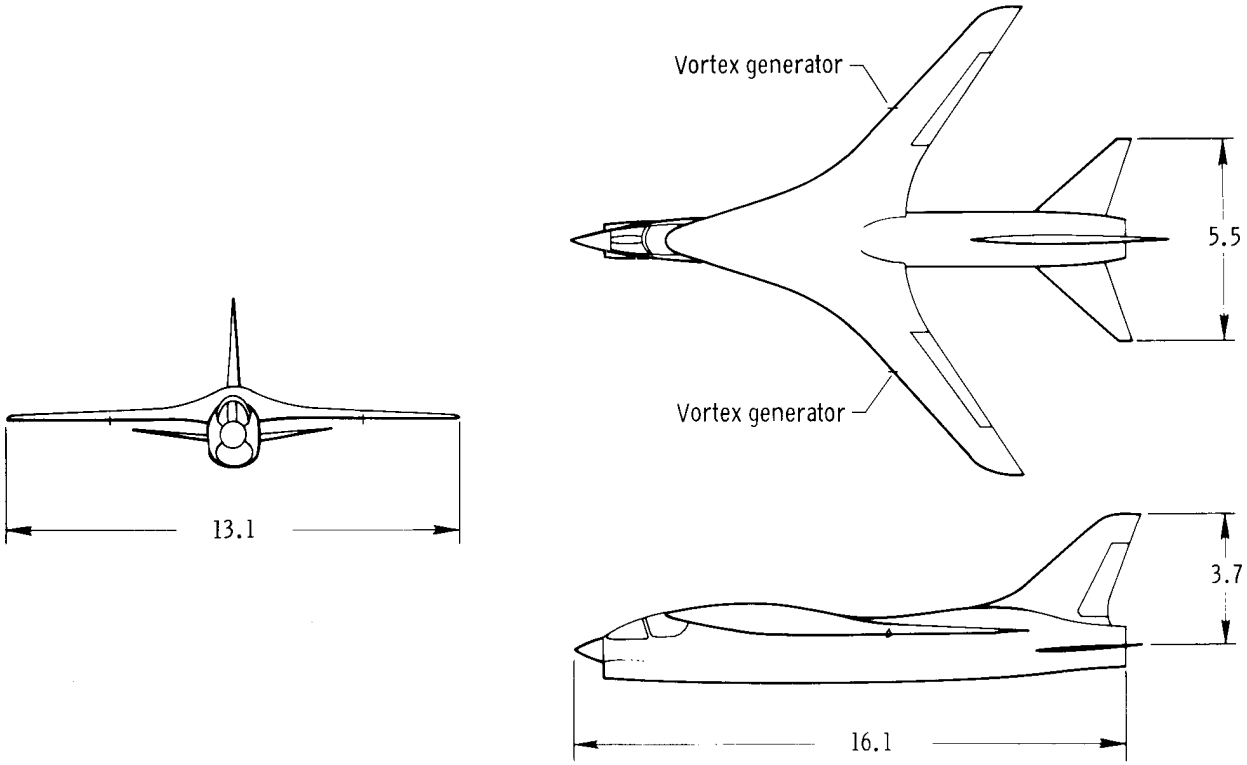

(b) Airplane dimensions (in meters).

Figure 1. F-8 supercritical wing airplane.

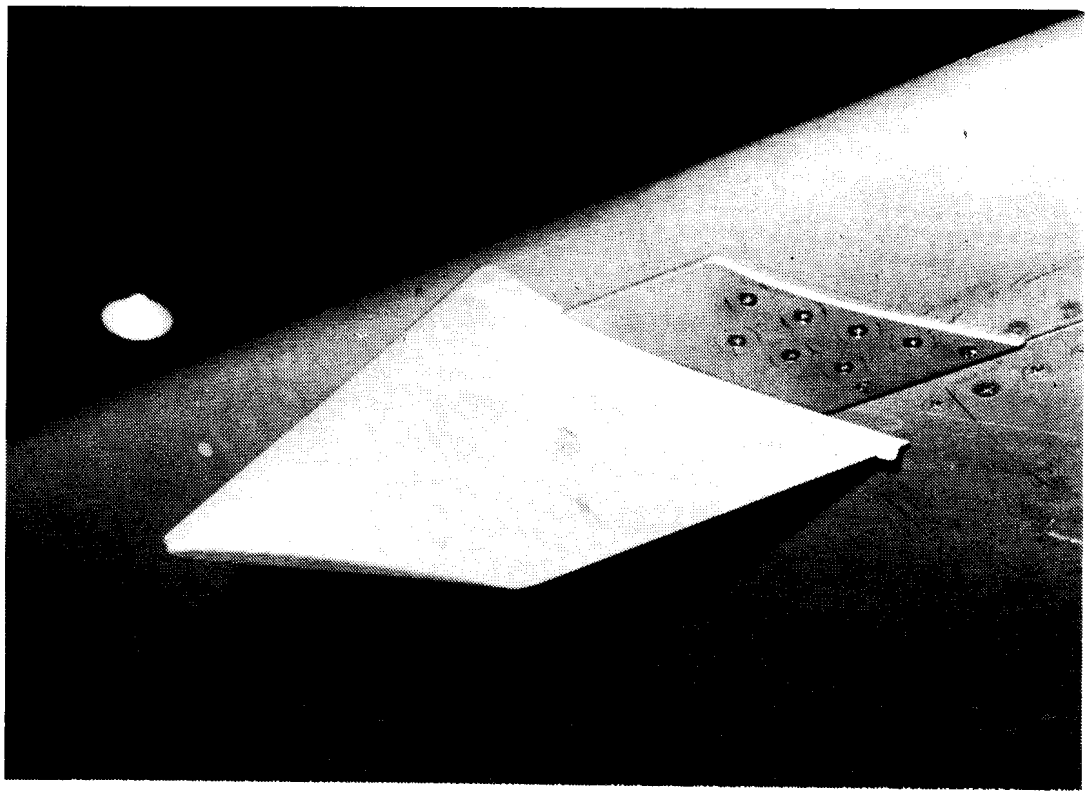

E-22709

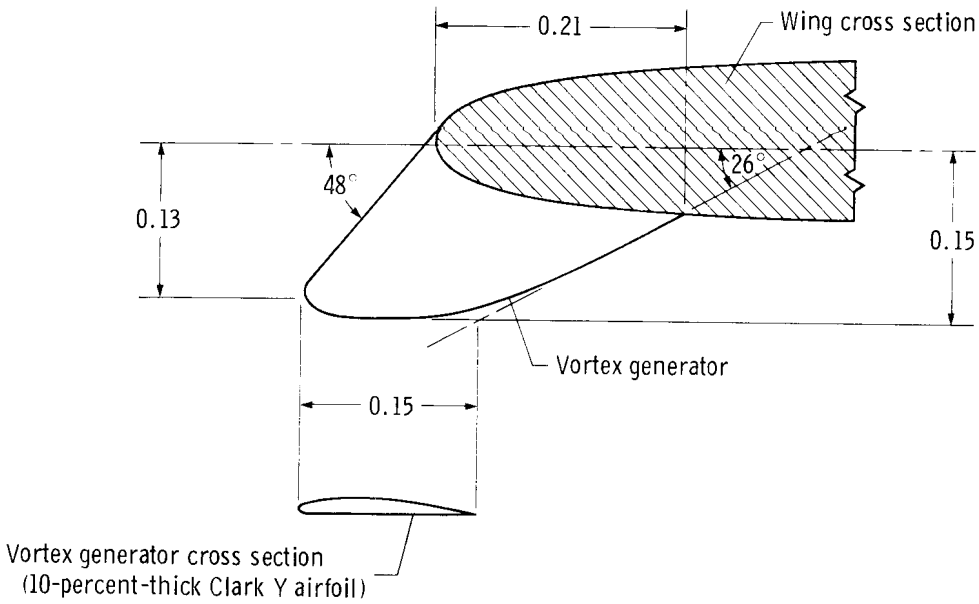

Figure 2. Vortex generator on bottom leading edge of wing. Dimensions are in meters.

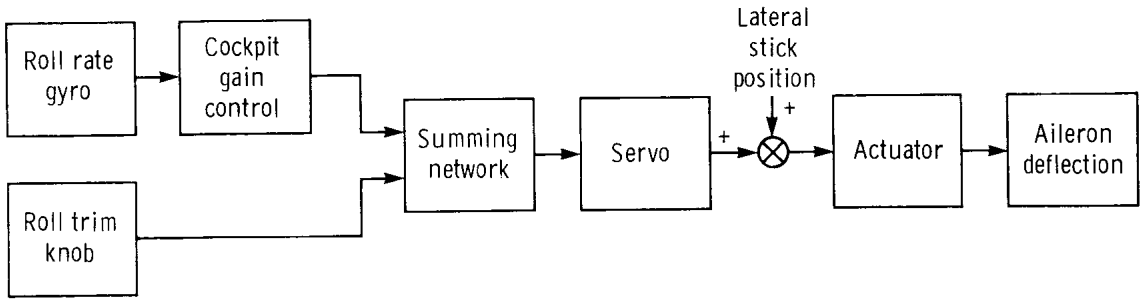

(a) Roll stability augmentation system.

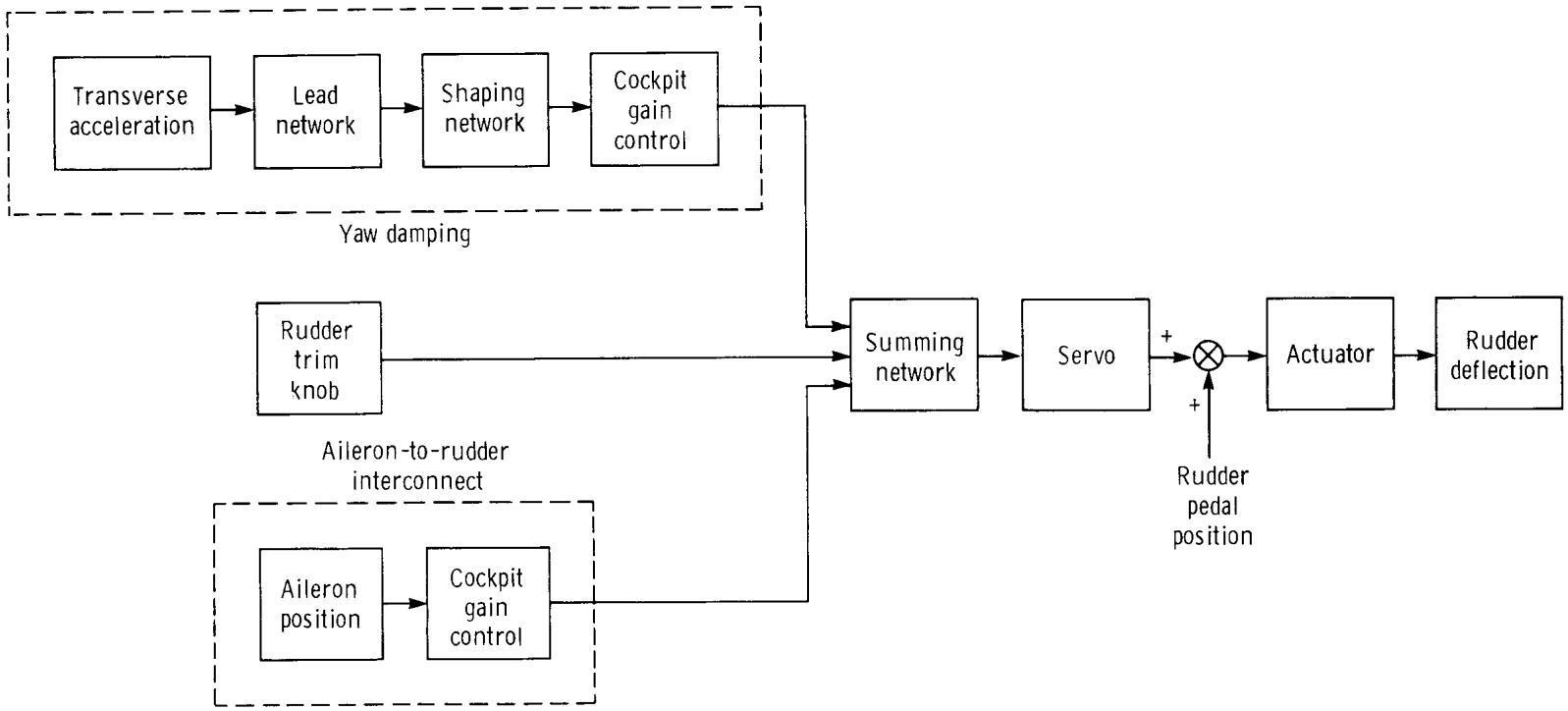

(b) Yaw stability augmentation system.

Figure 3. Modified control system.

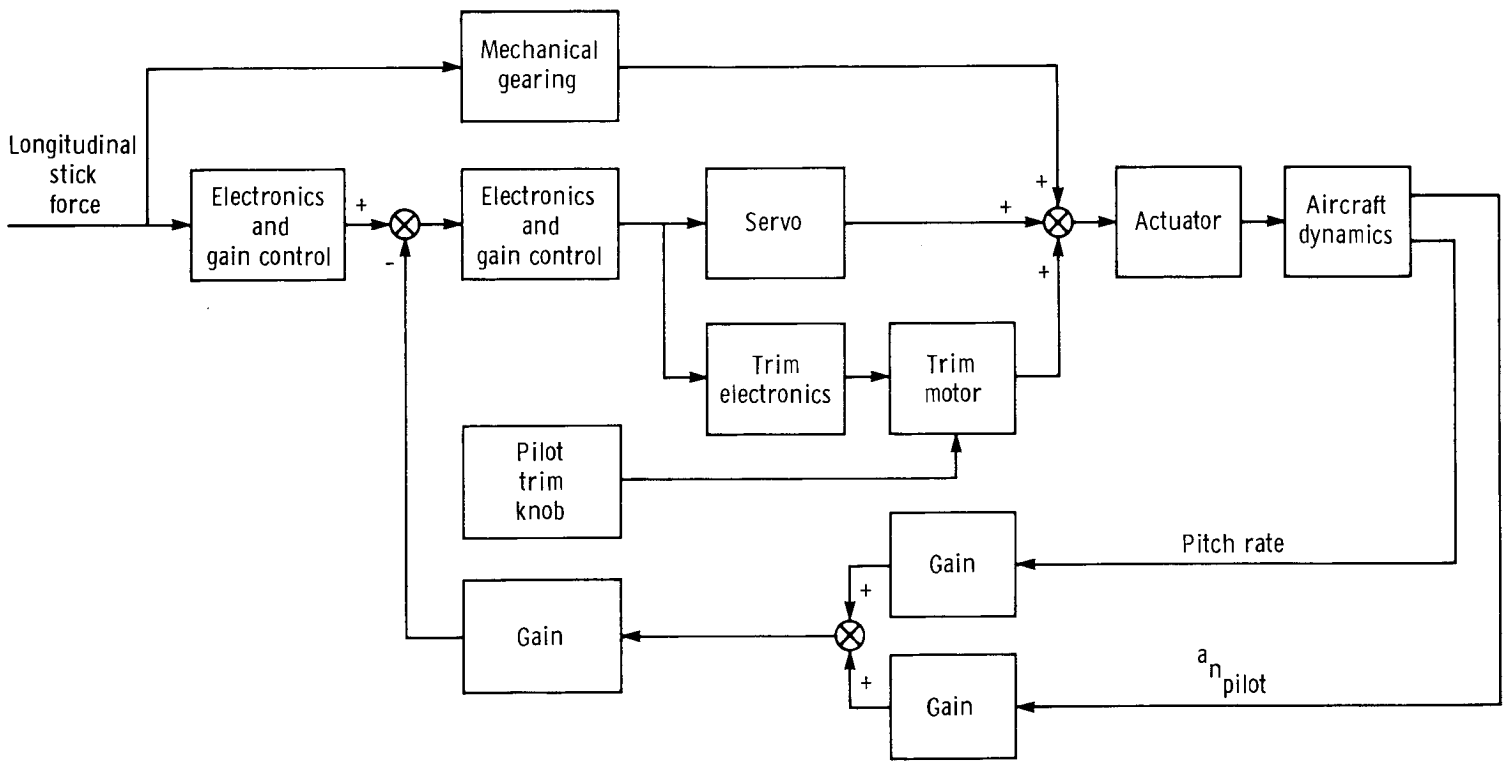

(c) Longitudinal command augmentation system.

Figure 3. Concluded.

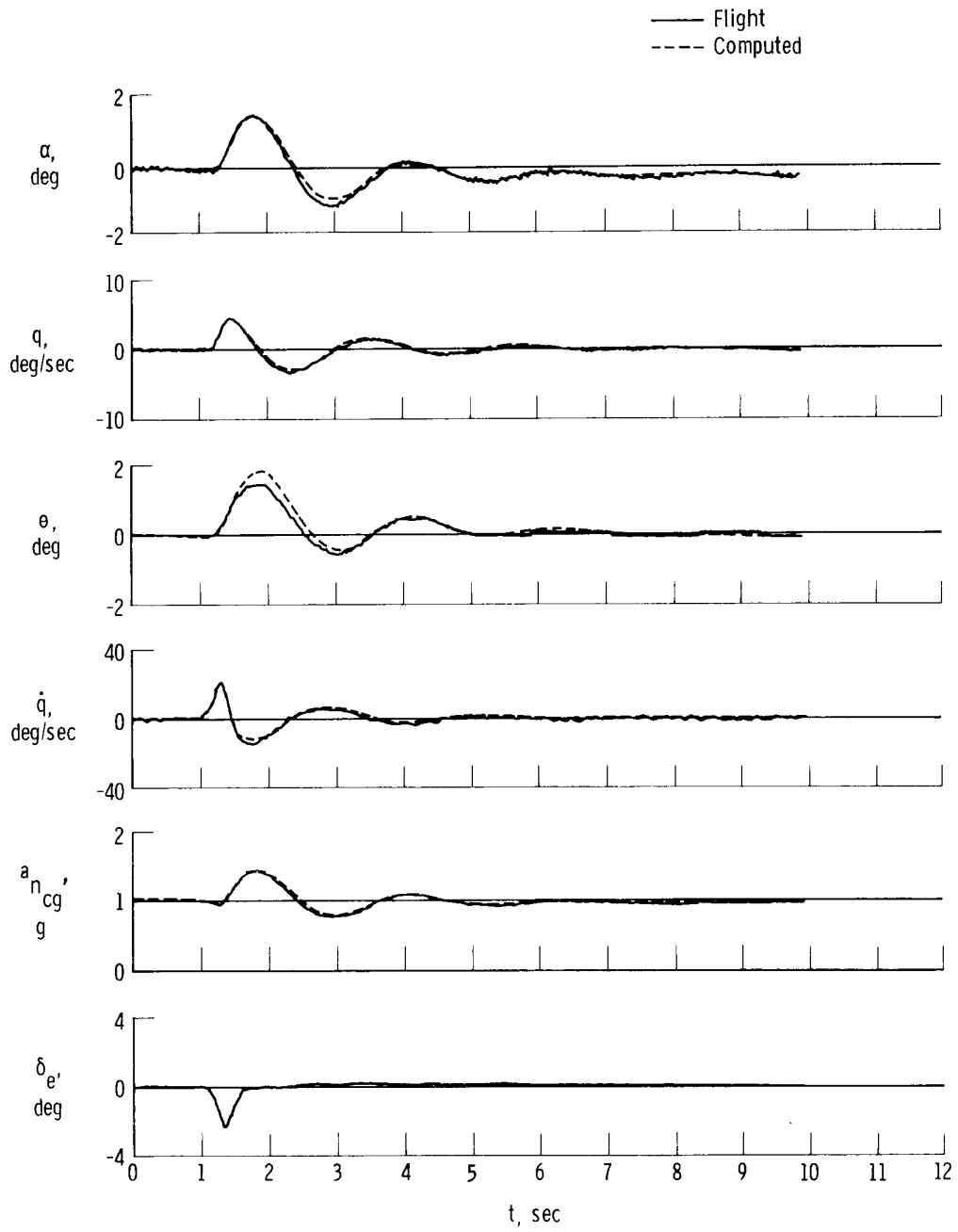

(a) Elevator pulse.

Figure 4. Typical matches of MMLE and flight data for maneuvers made to determine longitudinal derivatives.

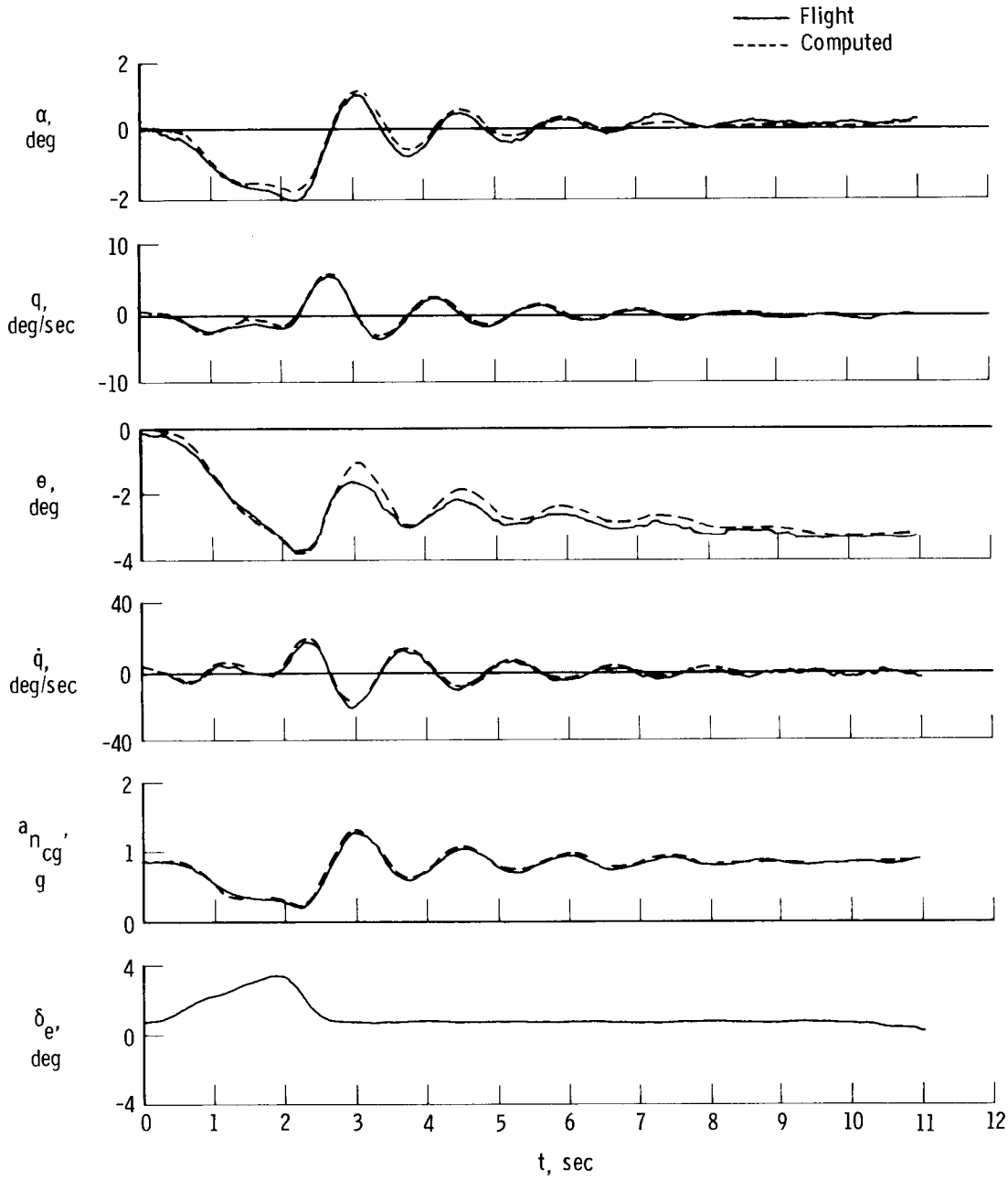

(b) Pushover.

Figure 4. Concluded.

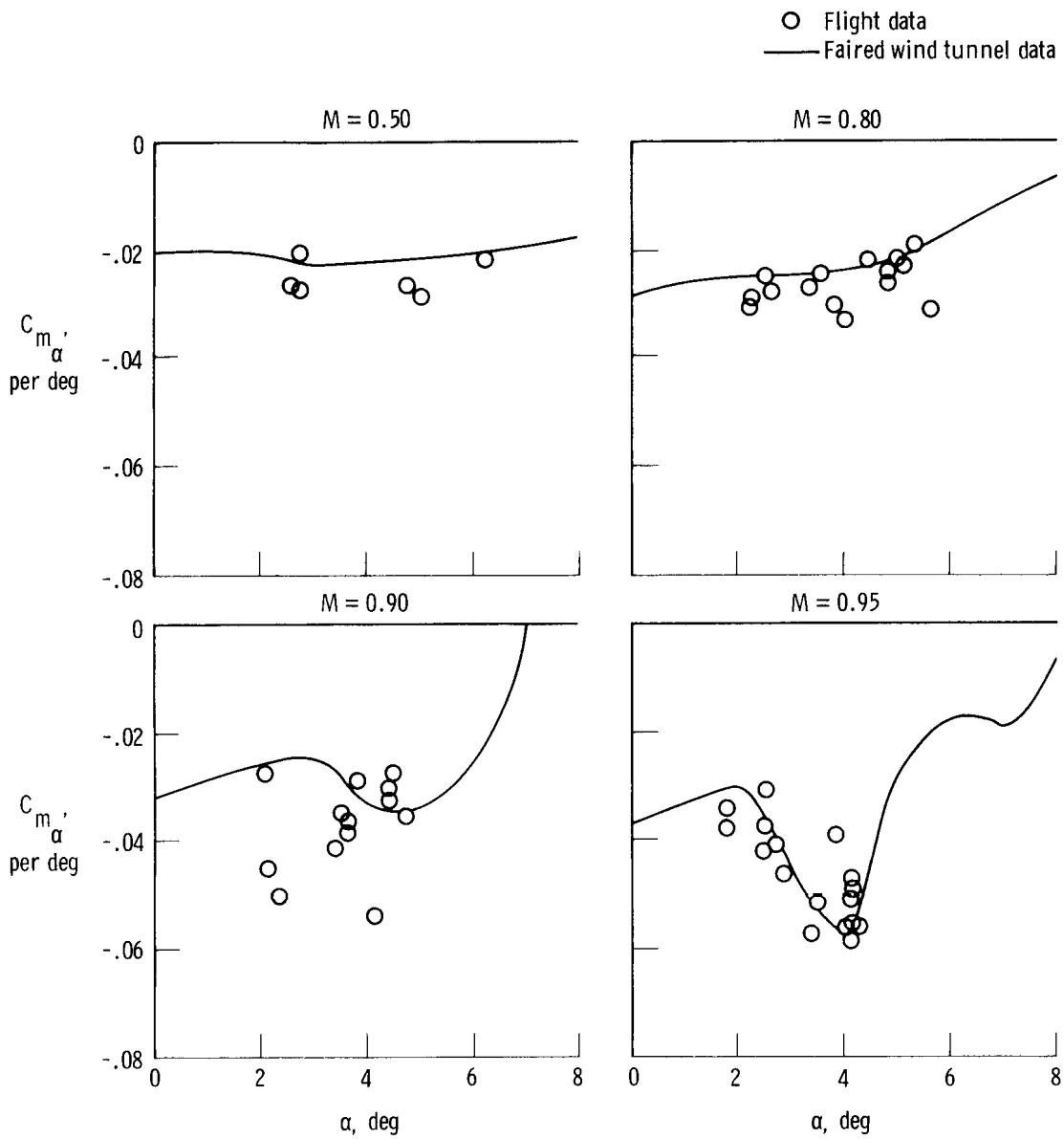

(a) C_{m_α}.

Figure 5. Variation of longitudinal derivatives with angle of attack.

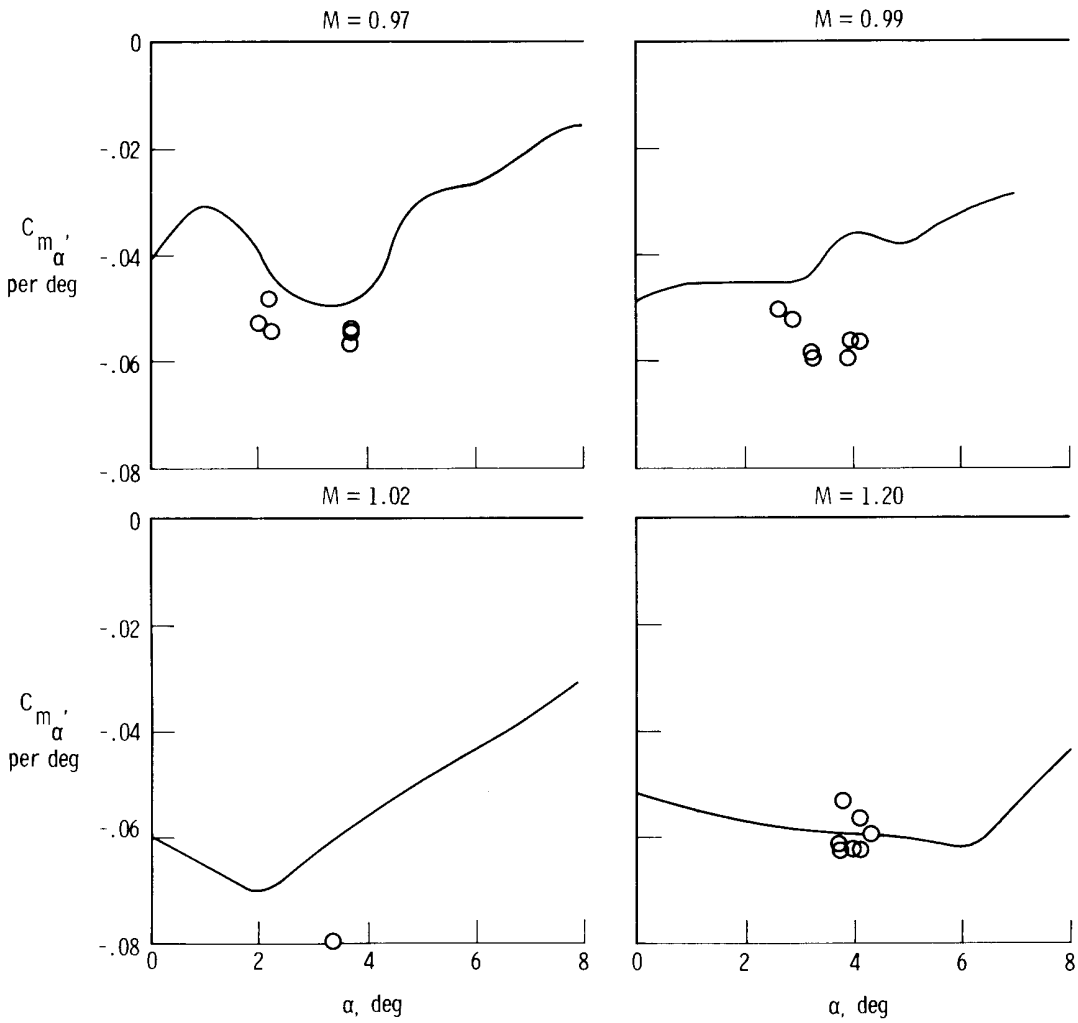

(a) Concluded.

Figure 5. Continued.

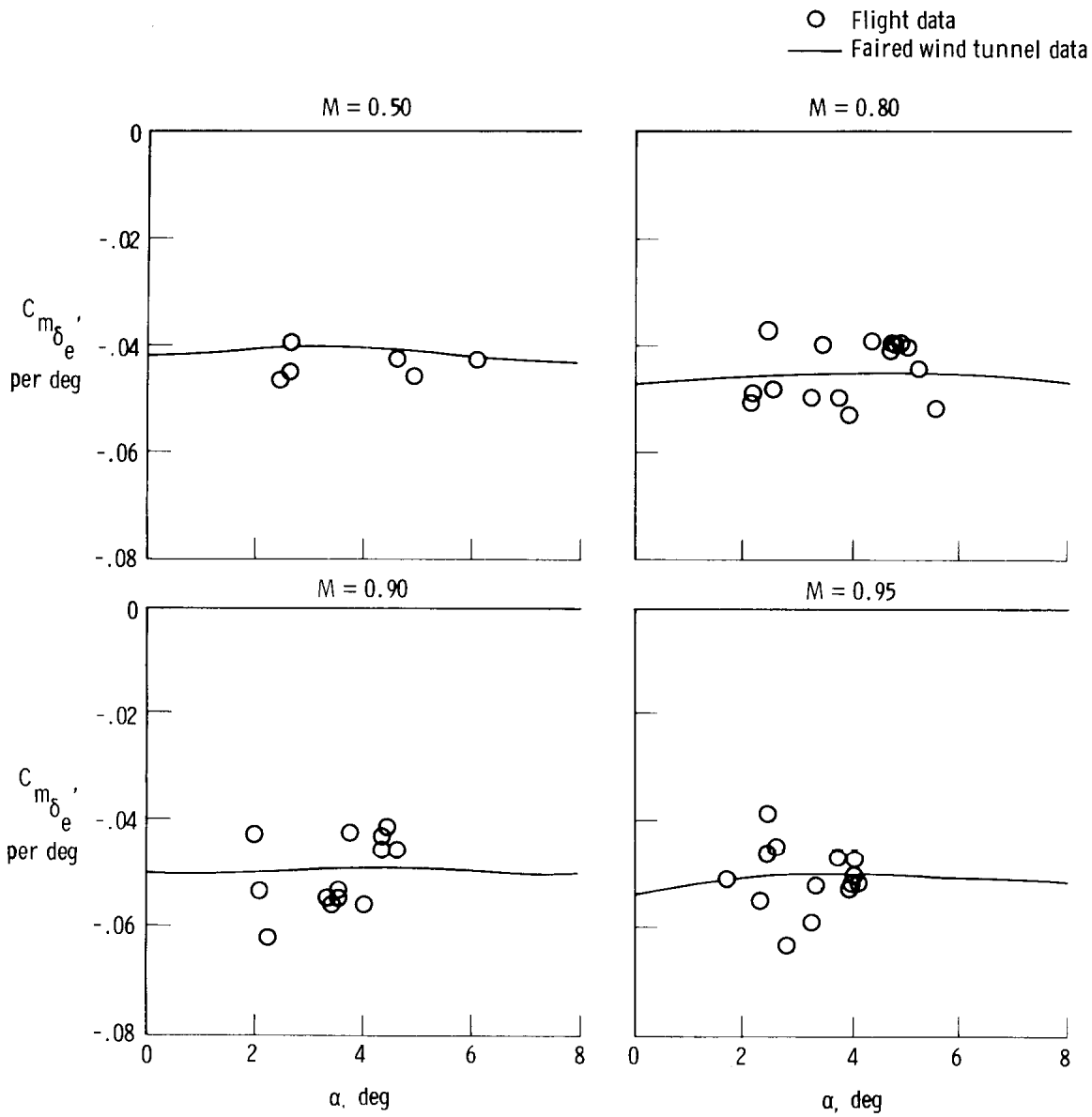

(b) $C_{m_{\delta_e}}$.

Figure 5. Continued.

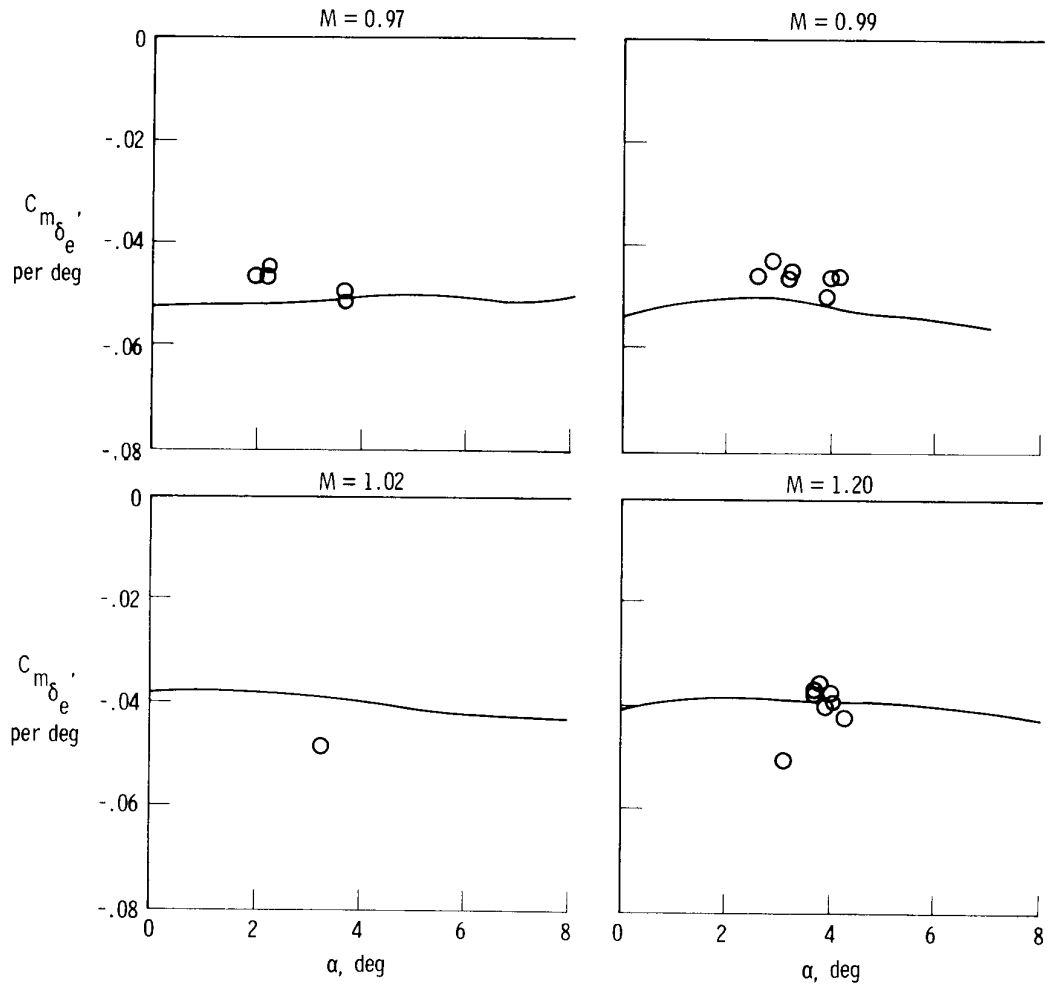

(b) Concluded.

Figure 5. Continued.

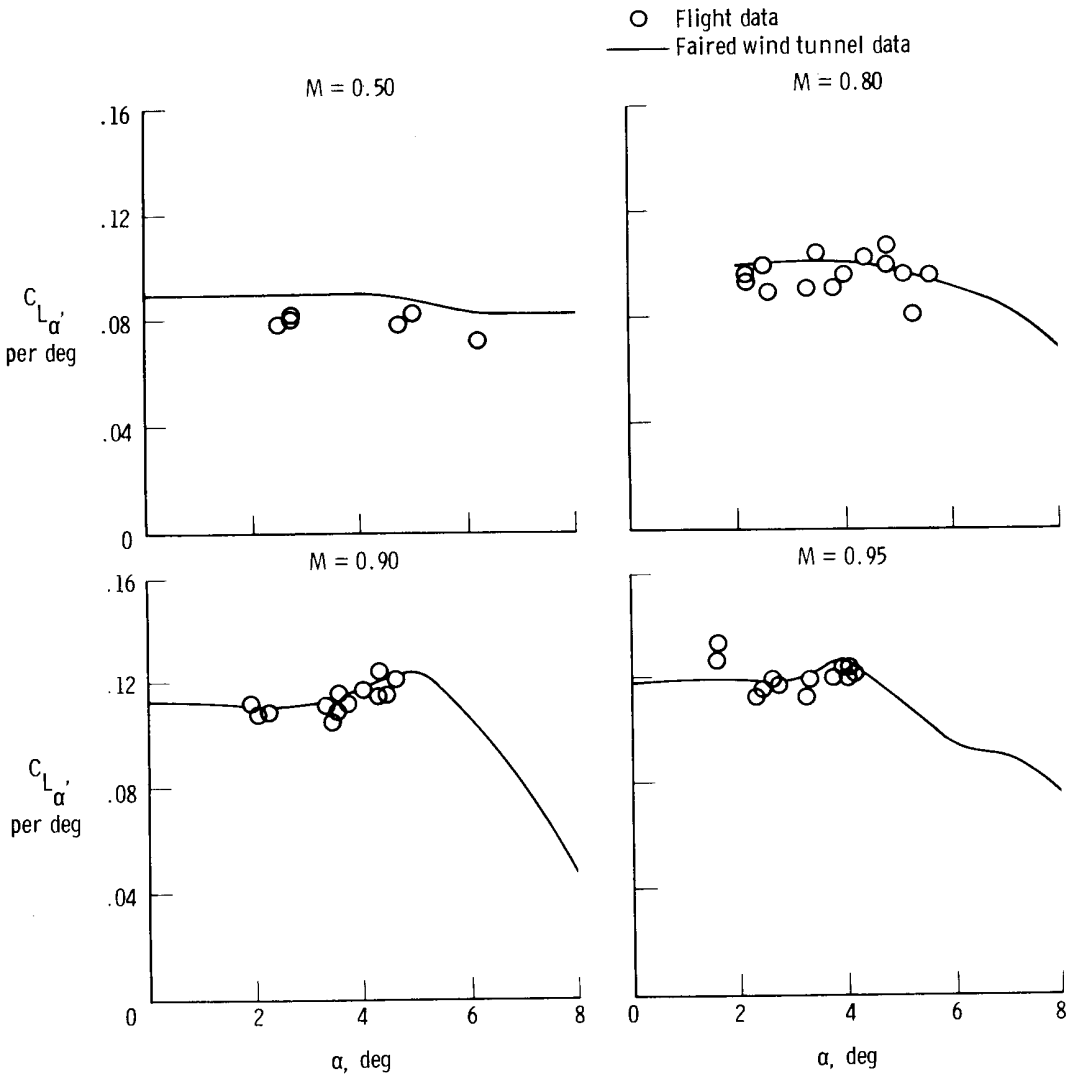

(c) C_{L_α}.

Figure 5. Continued.

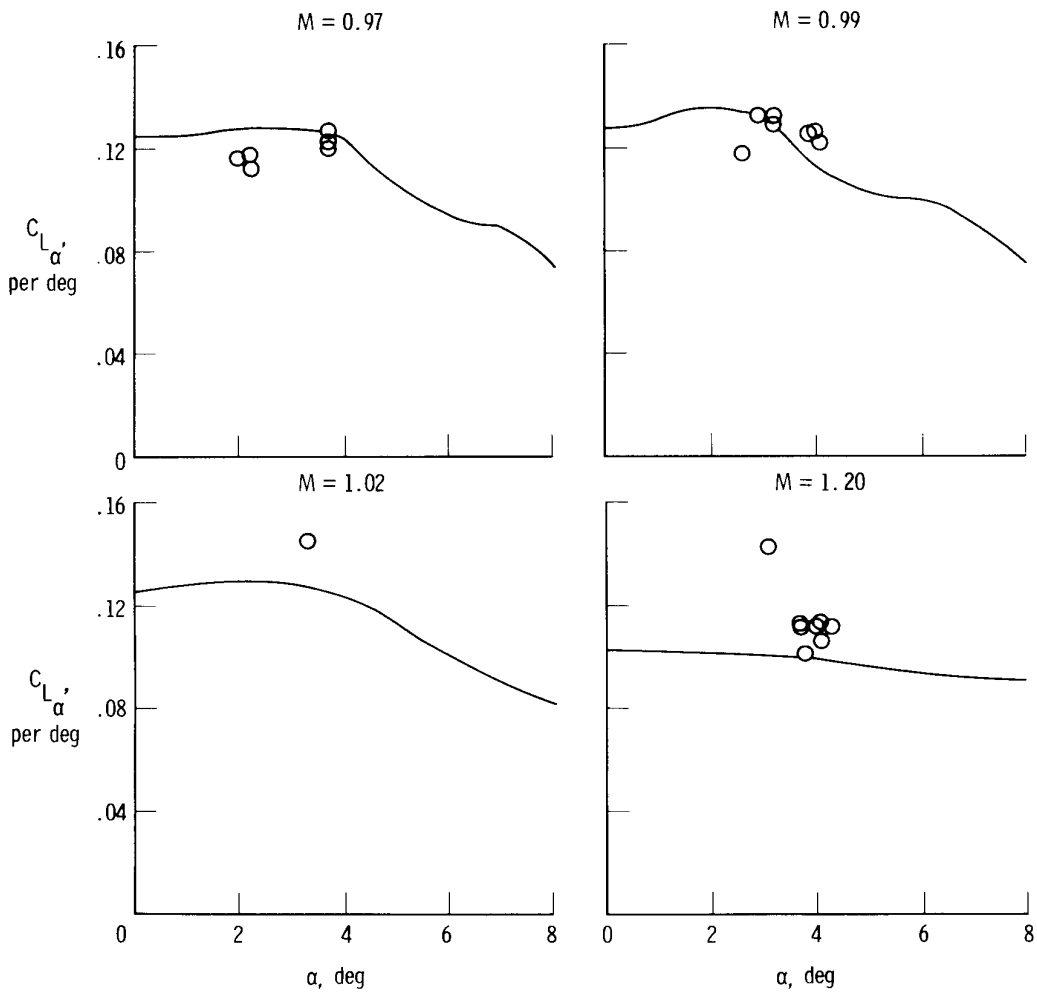

(c) Concluded.

Figure 5. Continued.

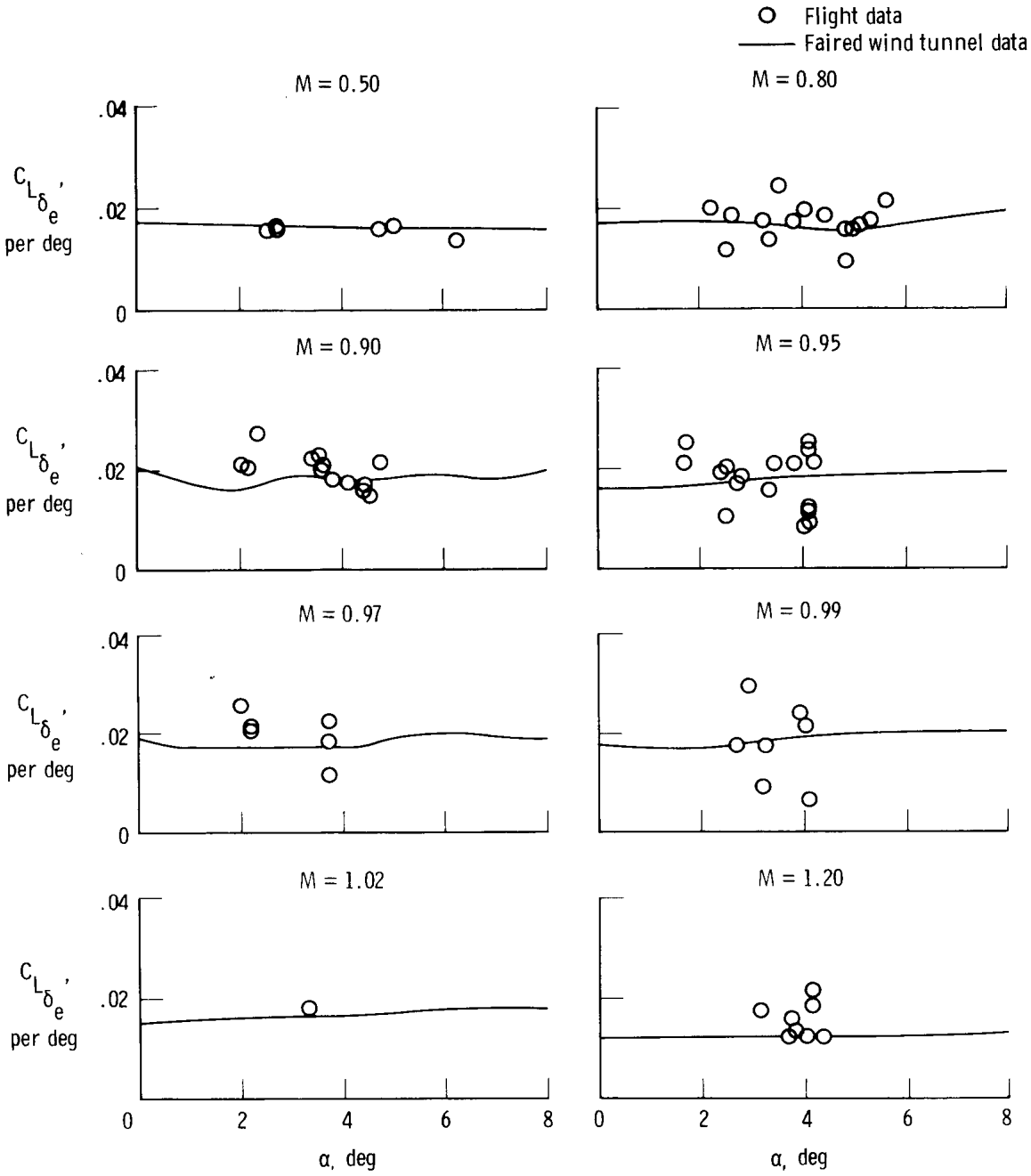

(d) $C_{L_{\delta_e}}$.

Figure 5. Continued.

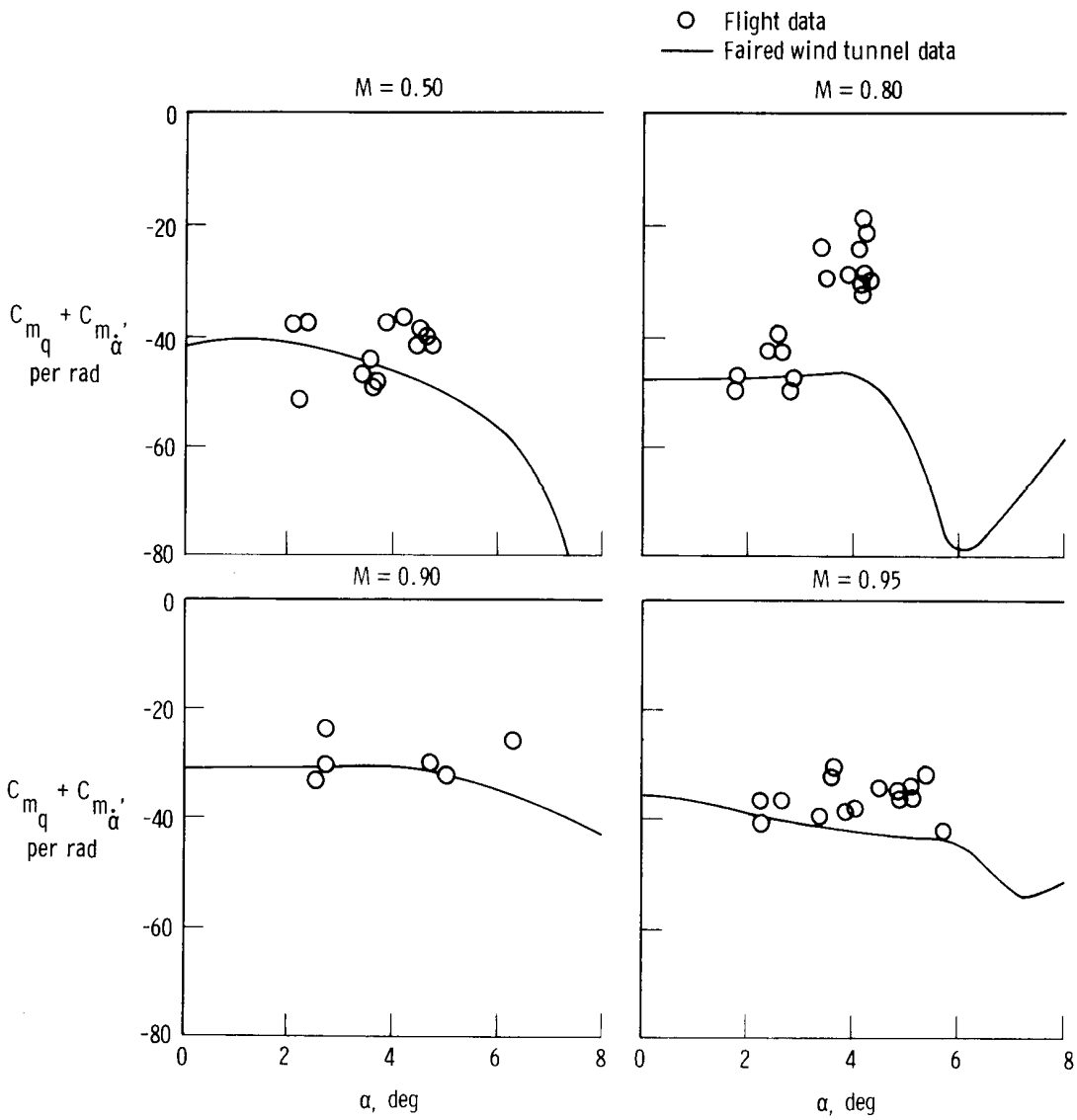

(e) $C_{m_q} + C_{m_{\dot{\alpha}}}$.

Figure 5. Continued.

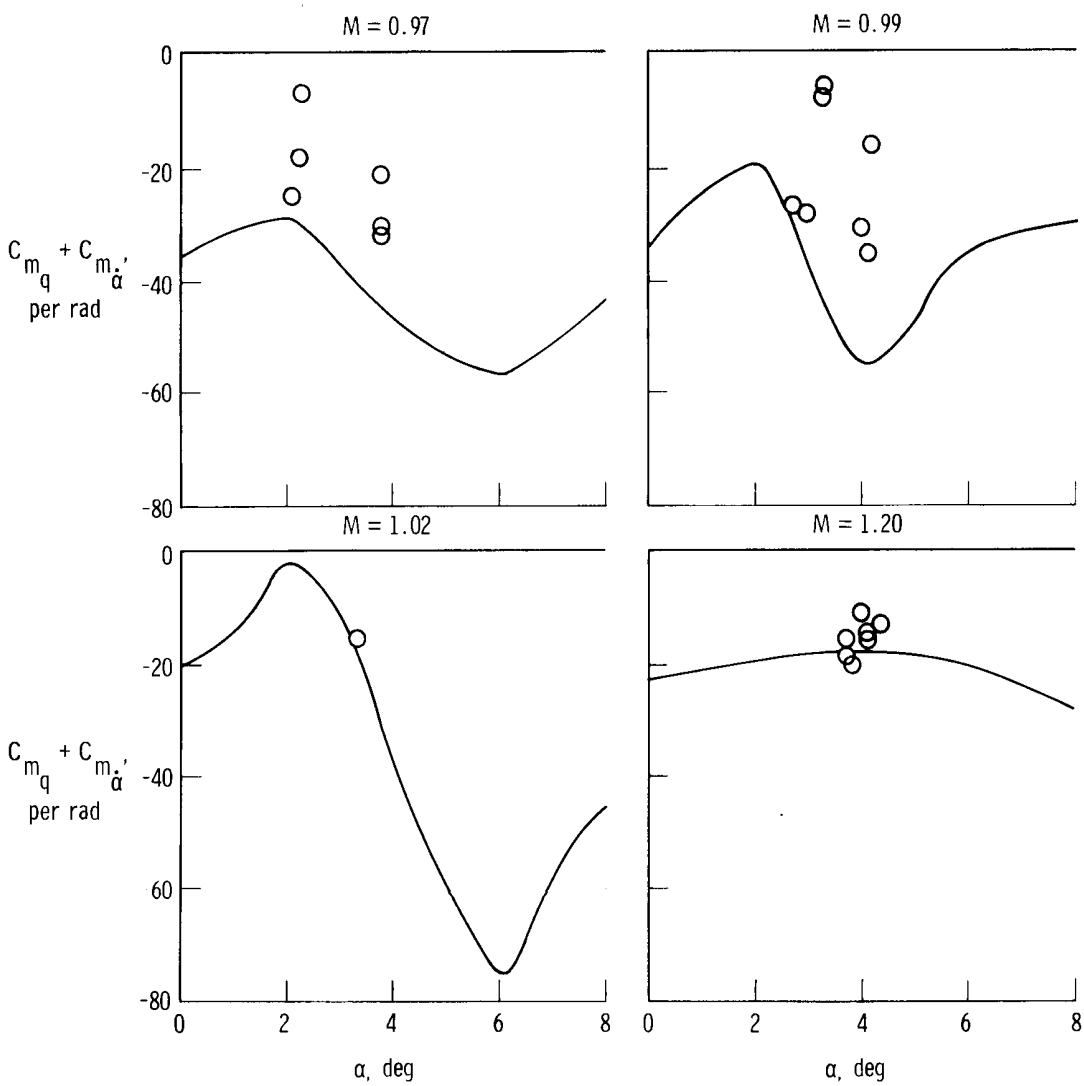

(e) Concluded.

Figure 5. Concluded.

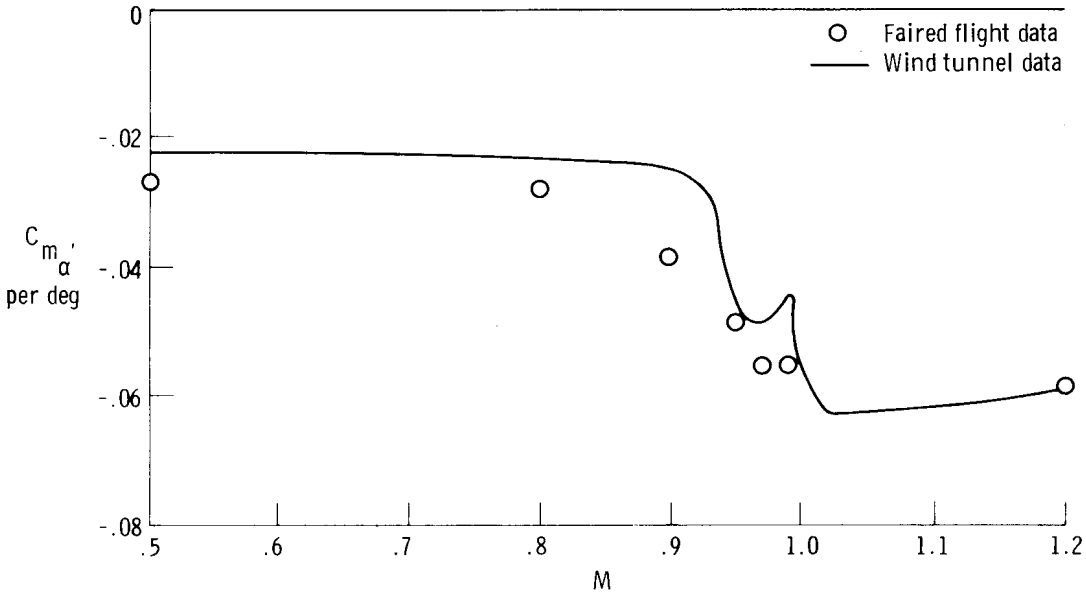

(a) C_{m_α}.

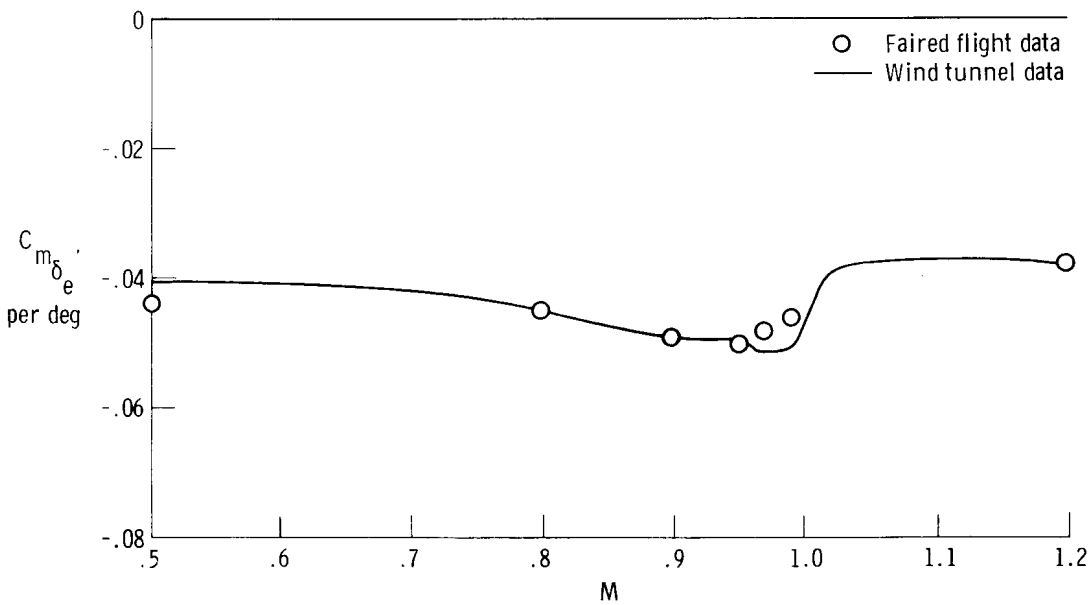

(b) $C_{m_{\delta_e}}$.

Figure 6. Variation of longitudinal derivatives with Mach number at an angle of attack of 3°.

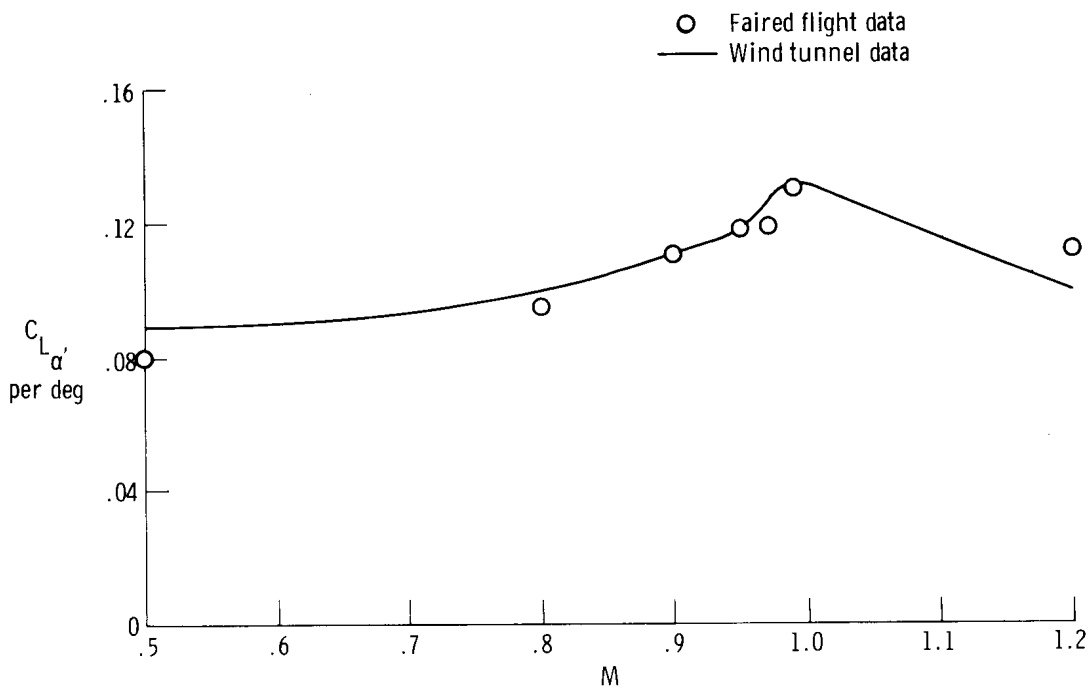

(c) C_{L_α}.

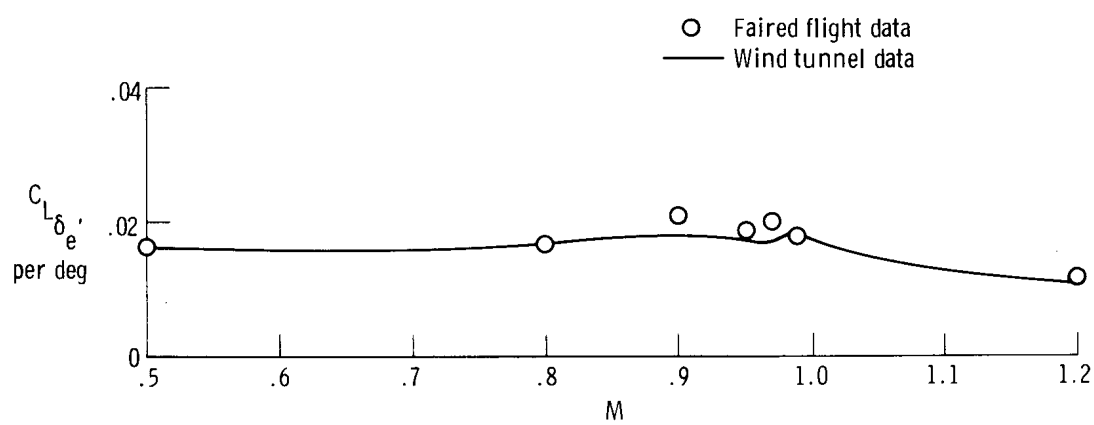

(d) $C_{L_{\delta_e}}$.

Figure 6. Continued.

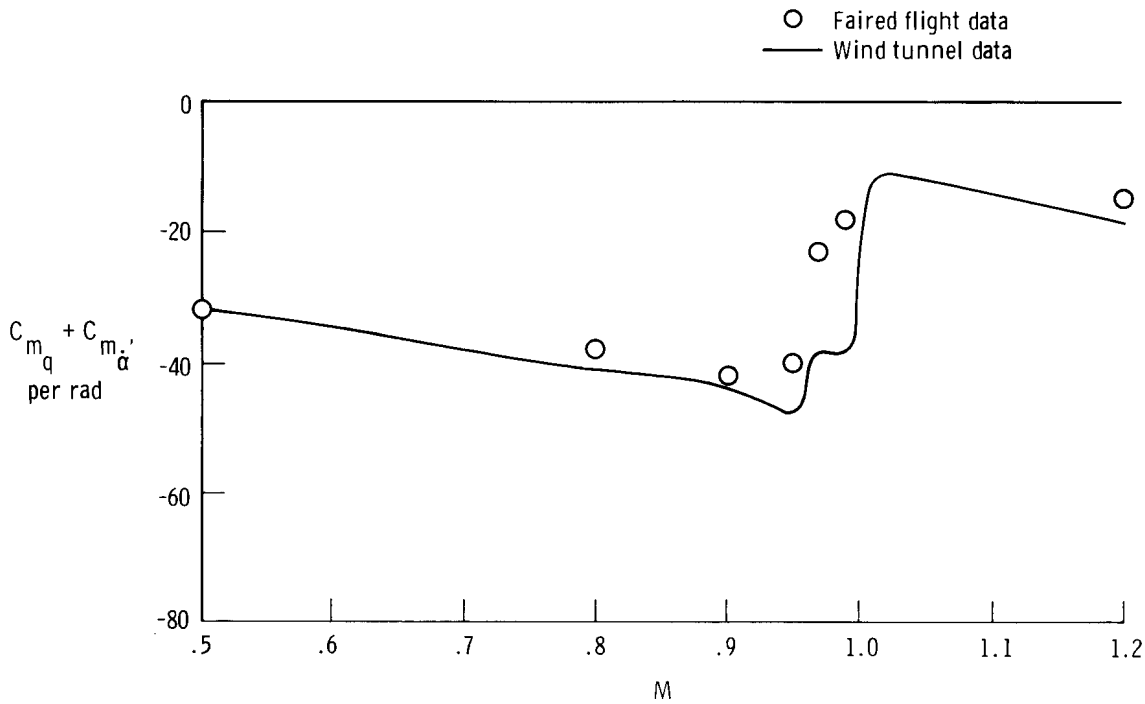

(e) $C_{m_q} + C_{m_{\dot{\alpha}}}$.

Figure 6. Concluded.

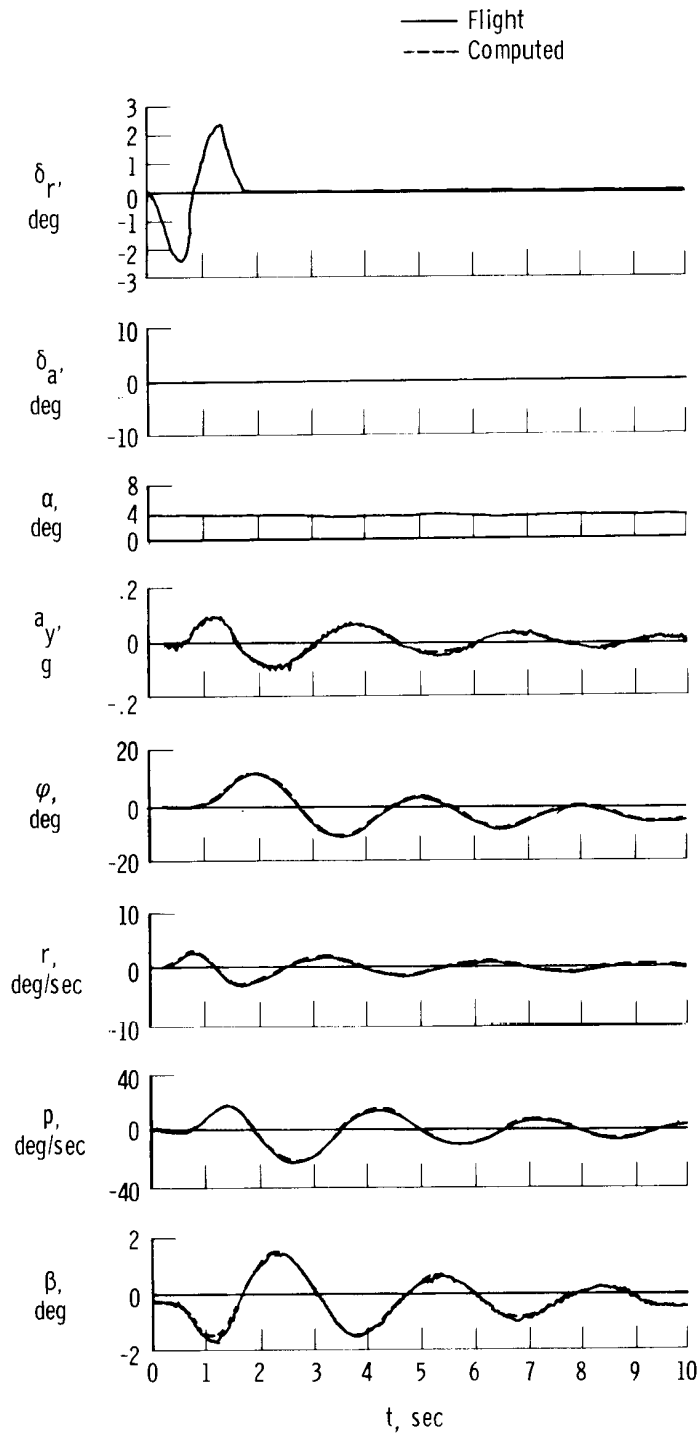

(a) Rudder doublet.

Figure 7. Typical matches of MMLE and flight data for maneuvers made to determine lateral-directional derivatives.

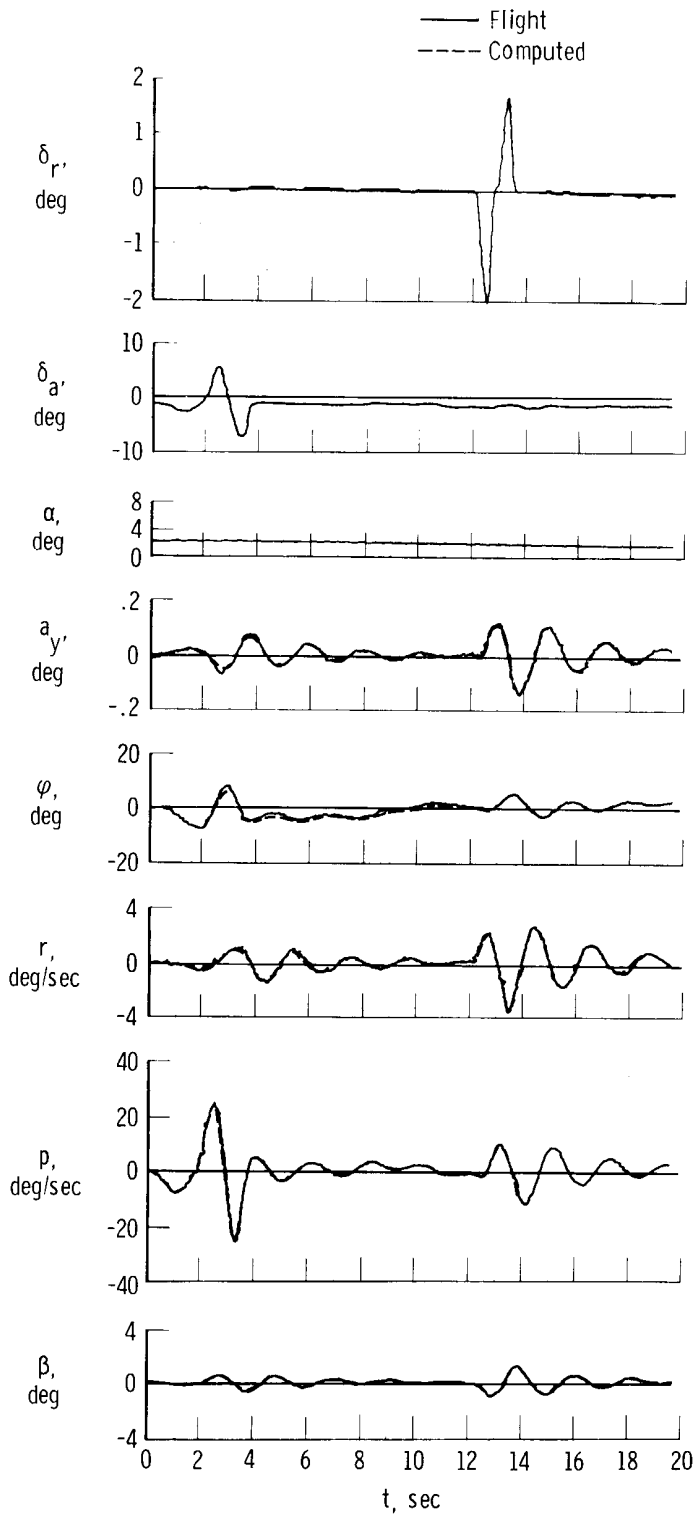

(b) Aileron doublet followed by rudder doublet.

Figure 7. Concluded.

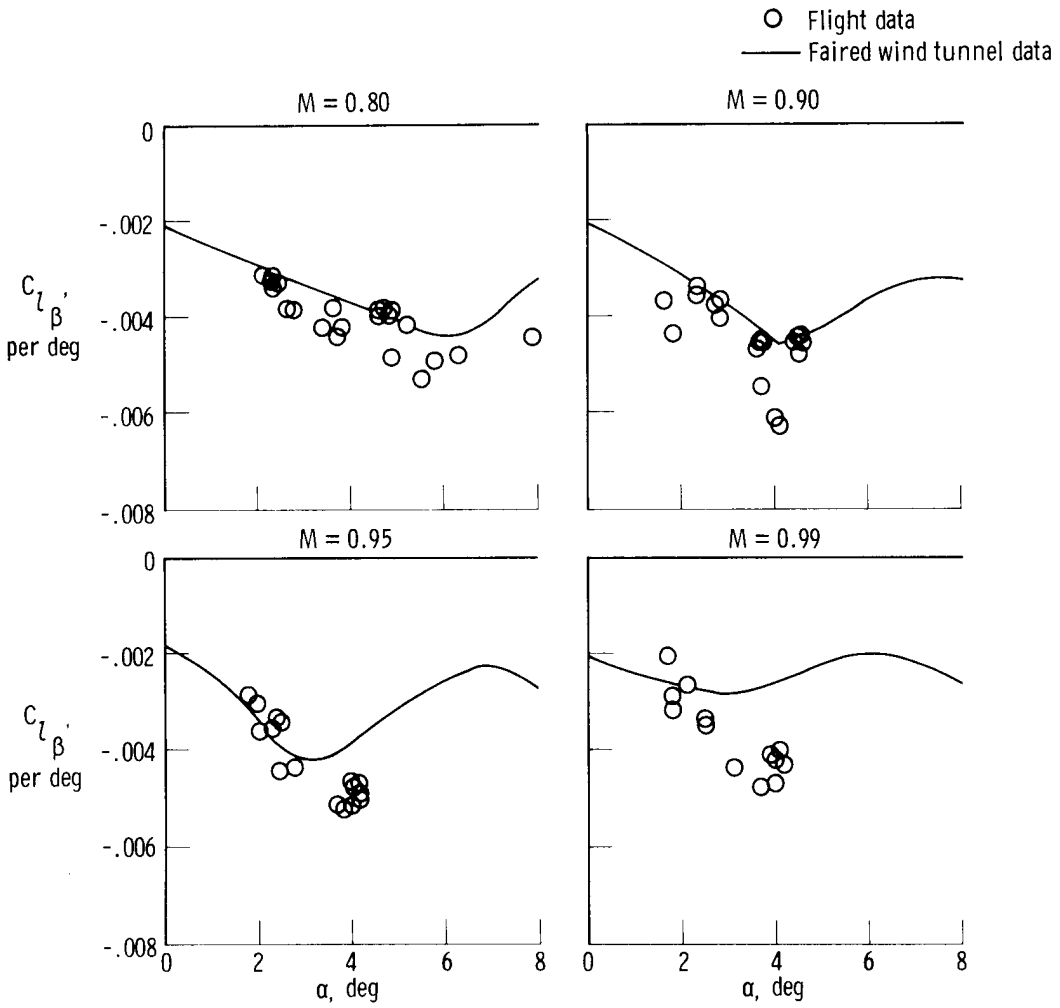

(a) C_{l_β}.

Figure 8. Lateral-directional derivatives as a function of angle of attack.

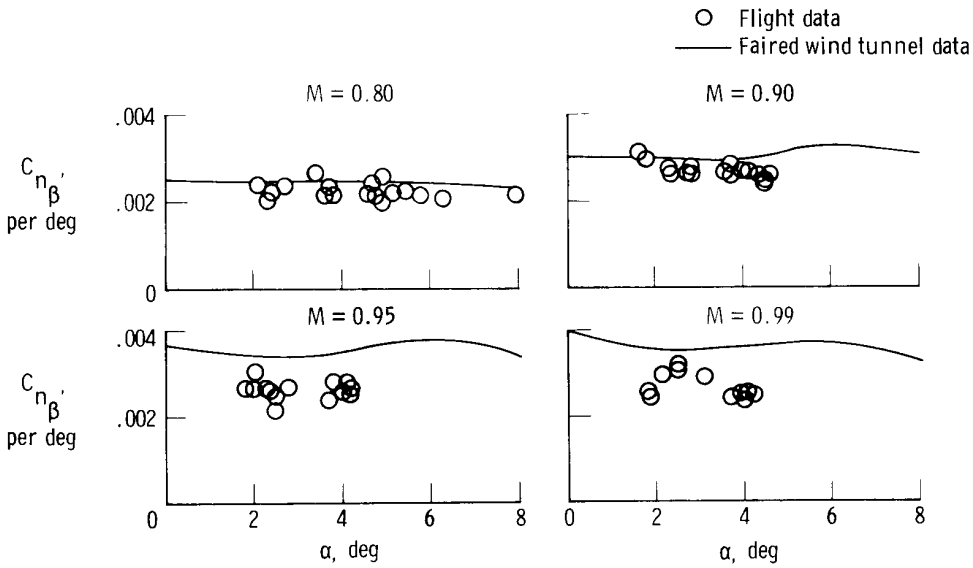

(b) C_{n_β}.

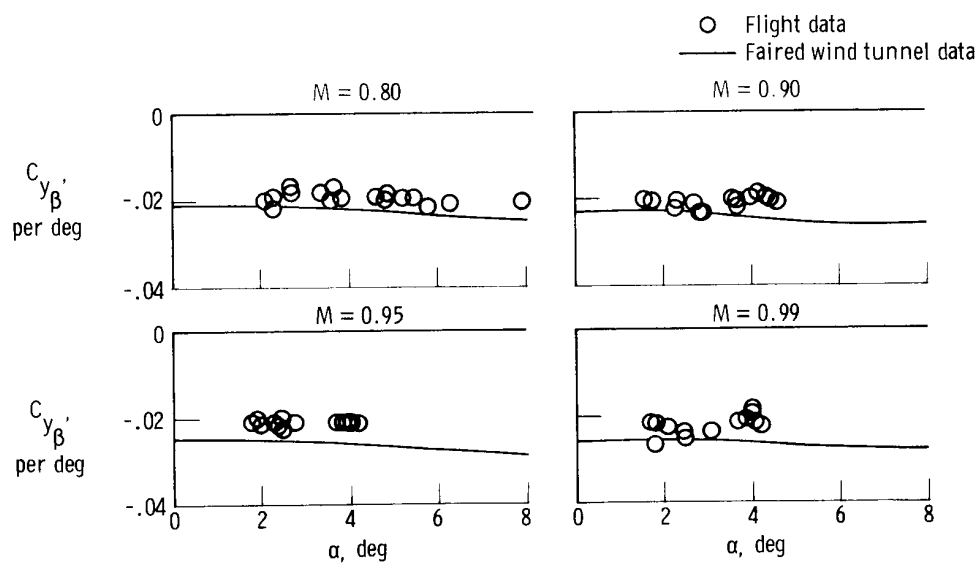

(c) C_{y_β}.

Figure 8. Continued.

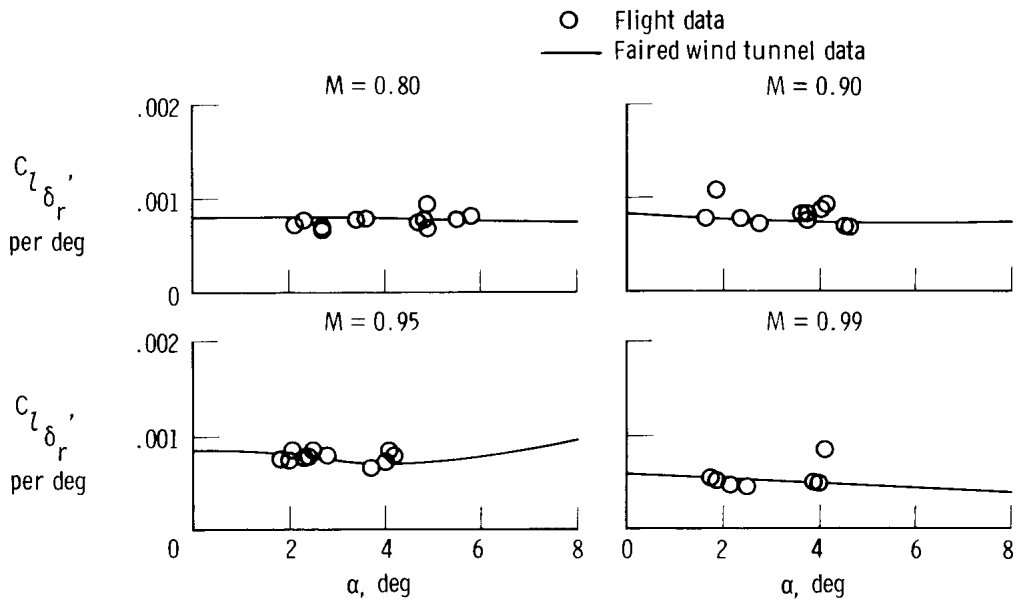

(d) $C_{l_{\delta_r}}$.

Figure 8. Continued.

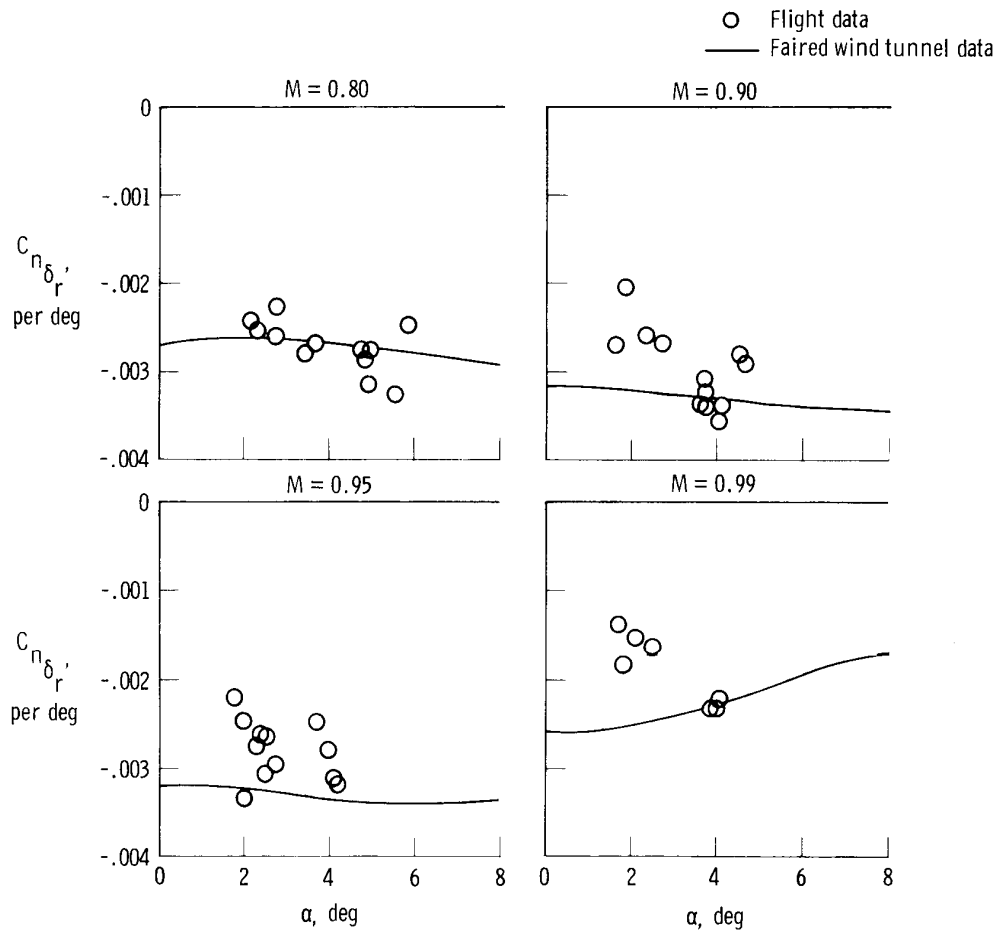

(e) $C_{n_{\delta_r}}$.

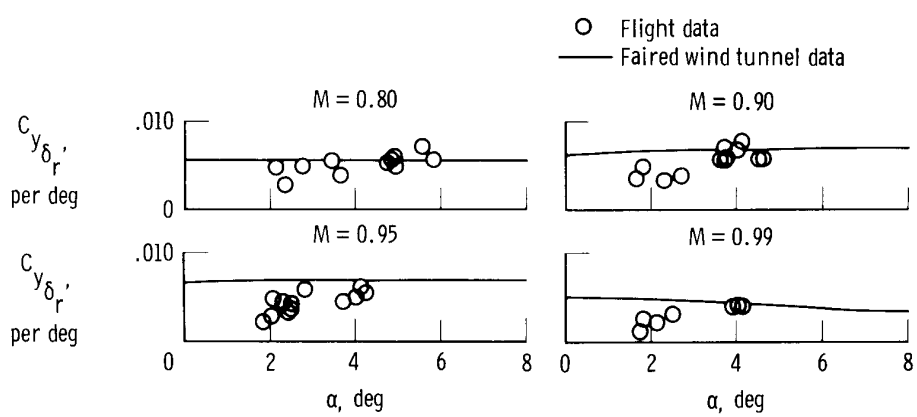

(f) $C_{y_{\delta_r}}$.

Figure 8. Continued.

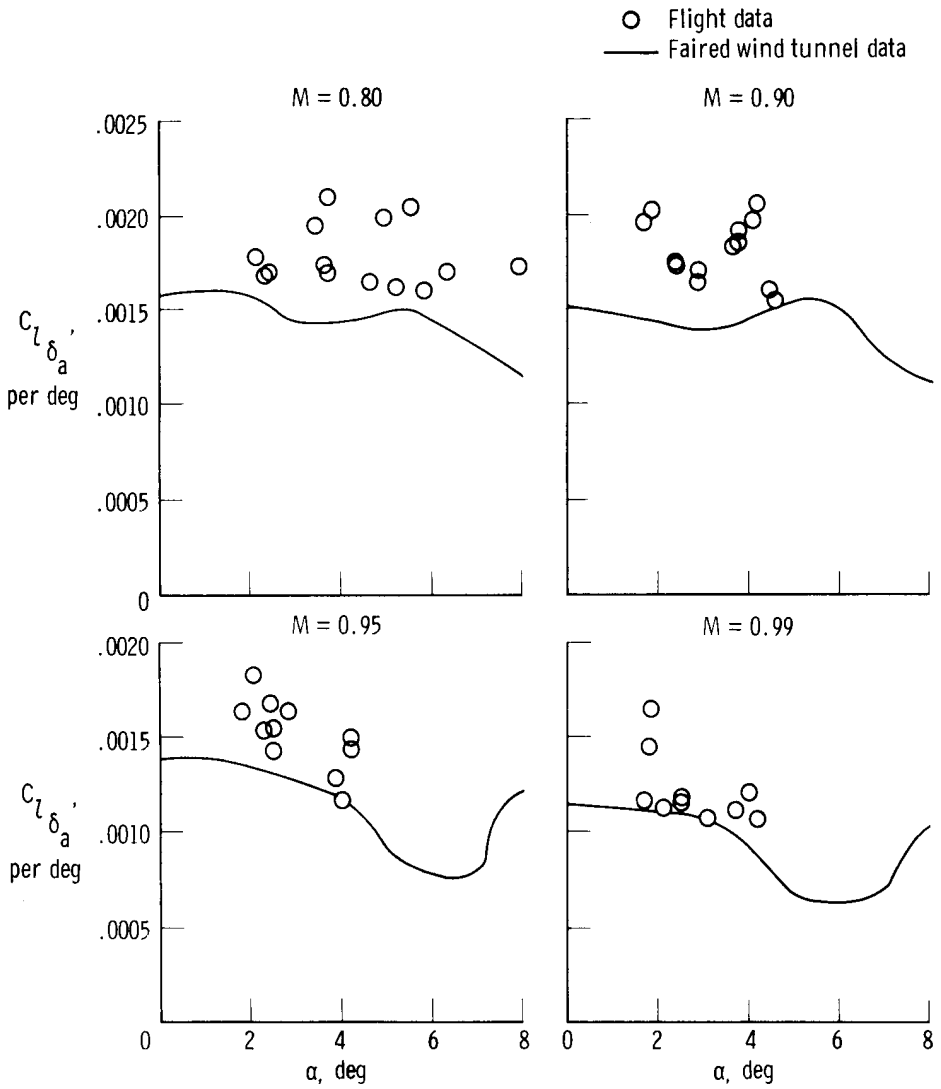

(g) $C_{l_{\delta_a}}$.

Figure 8. Continued.

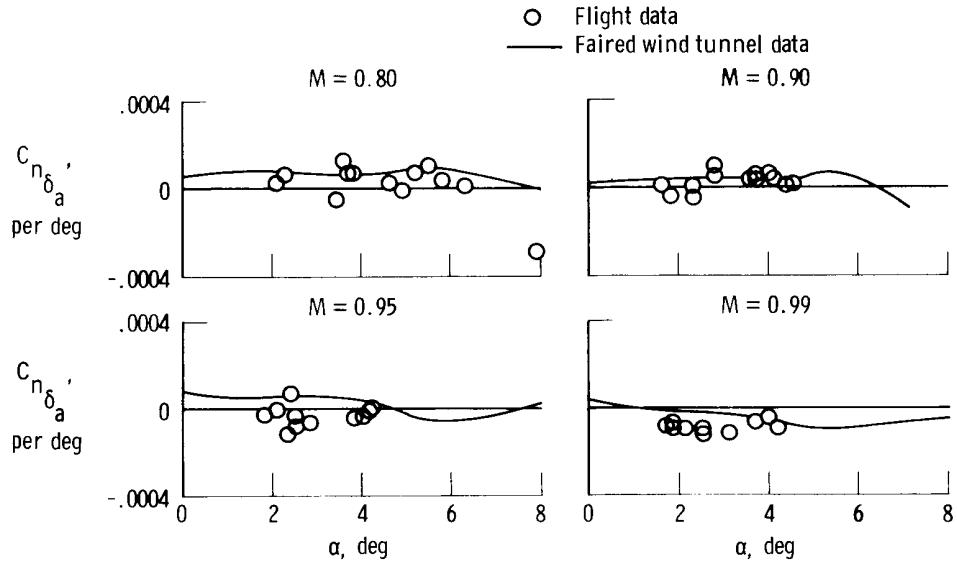

(h) $C_{n_{\delta_a}}$.

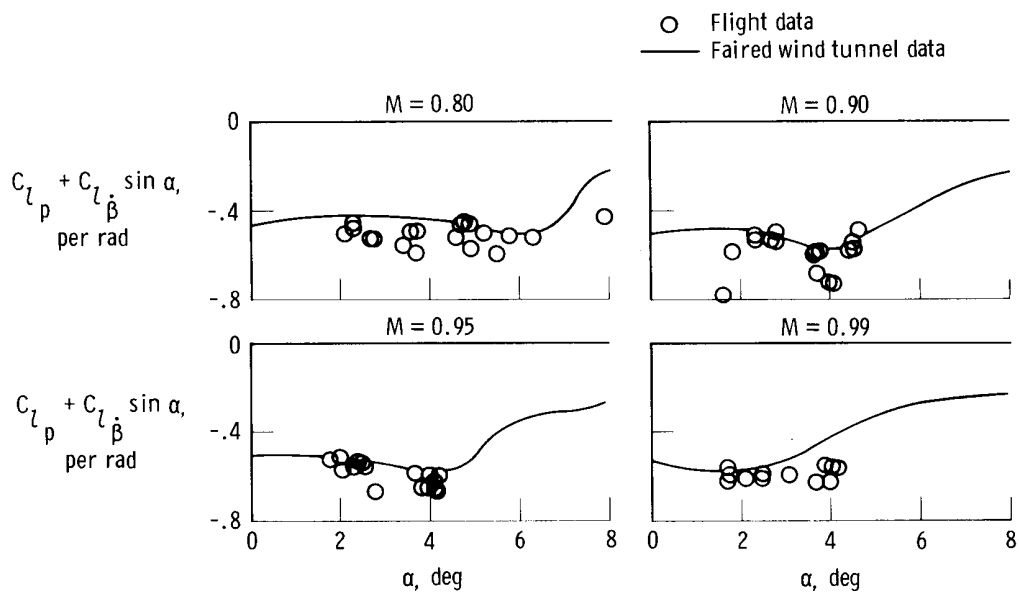

(i) $C_{l_p} + C_{l_{\dot{\beta}}} \sin \alpha$.

Figure 8. Continued.

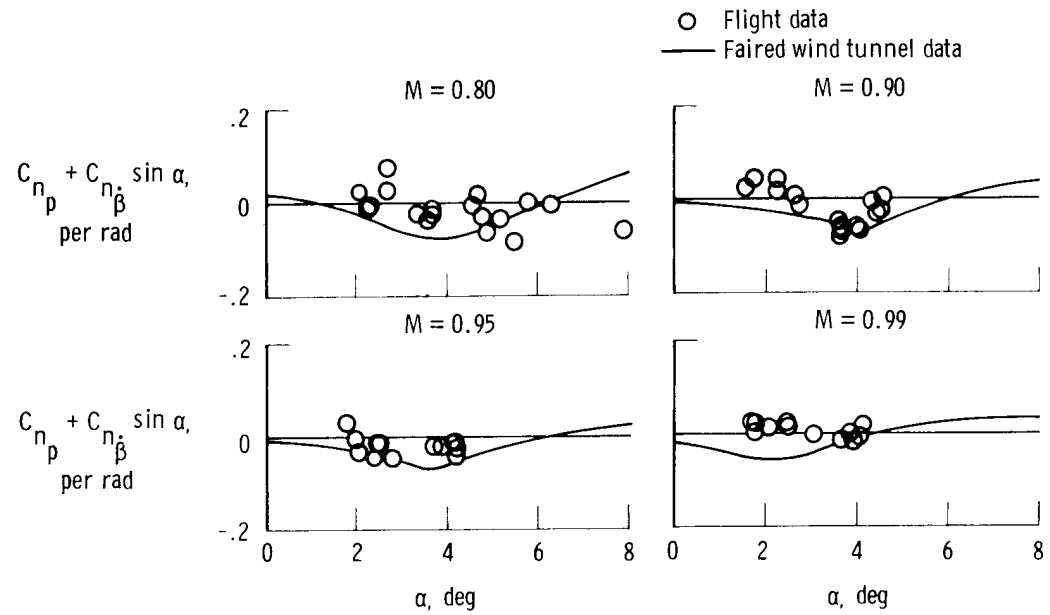

(j) $C_{n_p} + C_{n_{\dot{\beta}}} \sin \alpha$.

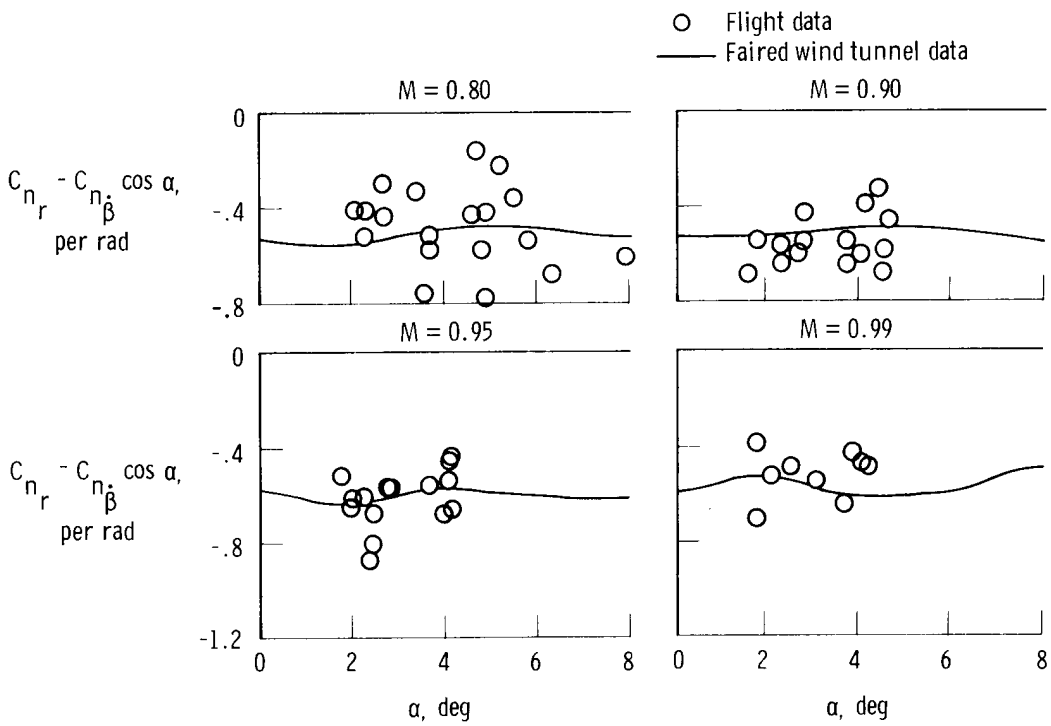

(k) $C_{n_r} - C_{n_{\dot{\beta}}} \cos \alpha$.

Figure 8. Concluded.

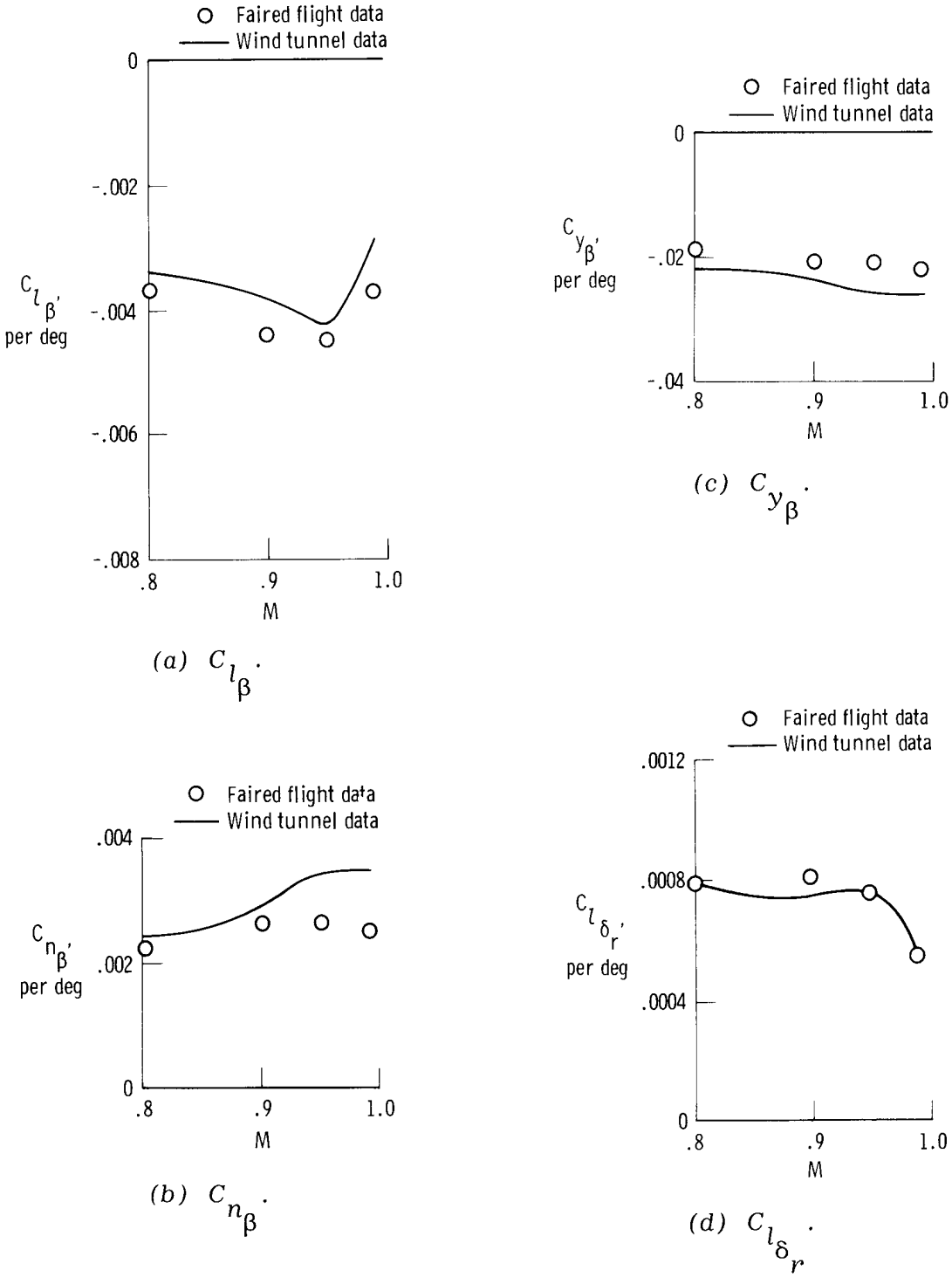

Figure 9. Variation of lateral-directional derivatives with Mach number at an angle of attack of 3°.

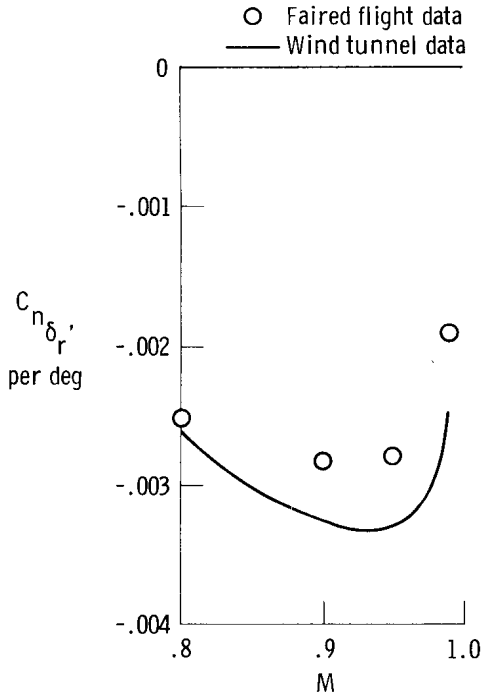

(e) $C_{n_{\delta_r}}$.

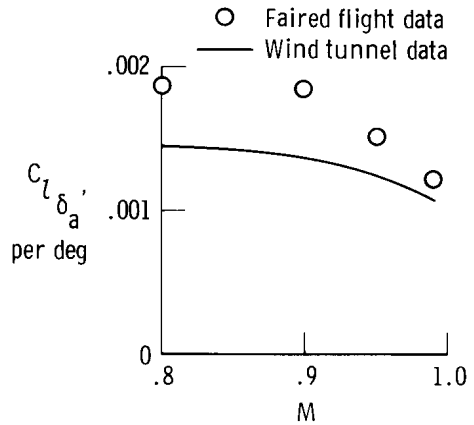

(g) $C_{l_{\delta_a}}$.

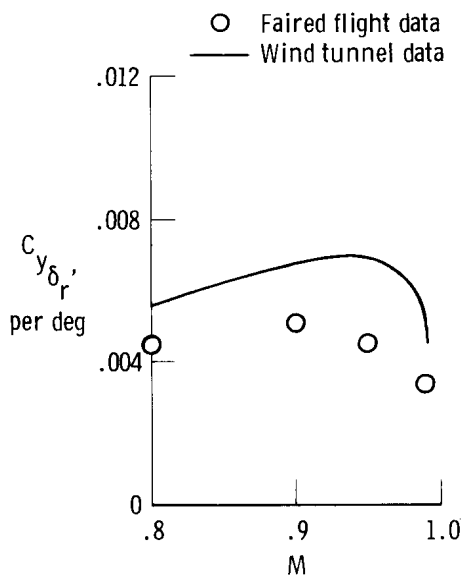

(f) $C_{y_{\delta_r}}$.

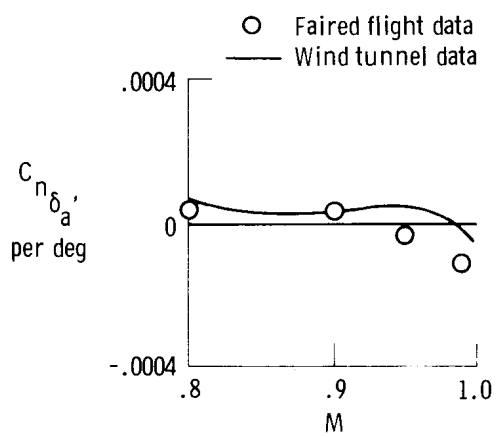

(h) $C_{n_{\delta_a}}$.

Figure 9. Continued.

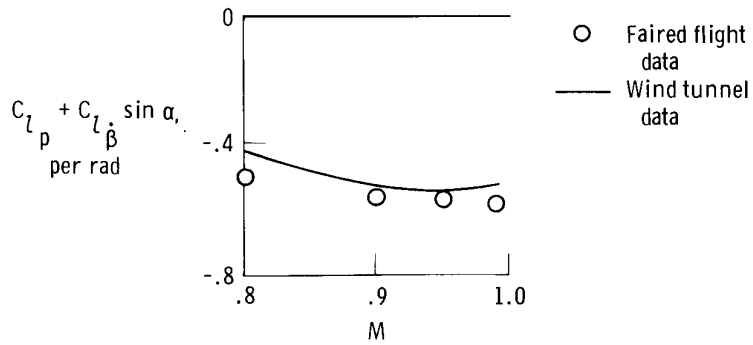

(i) $C_{l_p} + C_{l_{\dot{\beta}}} \sin \alpha$.

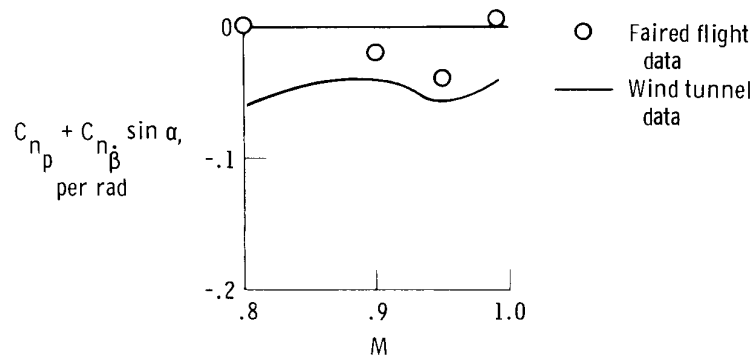

(j) $C_{n_p} + C_{n_{\dot{\beta}}} \sin \alpha$.

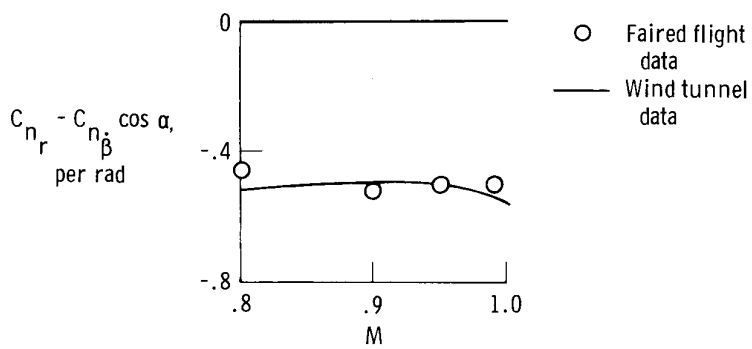

(k) $C_{n_r} - C_{n_{\dot{\beta}}} \cos \alpha$.

Figure 9. Concluded.

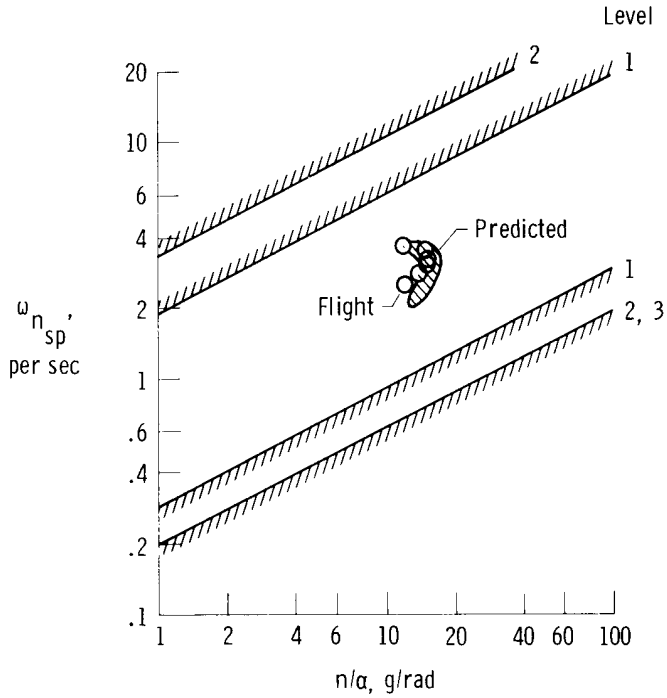

Figure 10. Comparison of flight and predicted values of longitudinal response with the requirements of reference 15. M = 0.80 to 1.20.

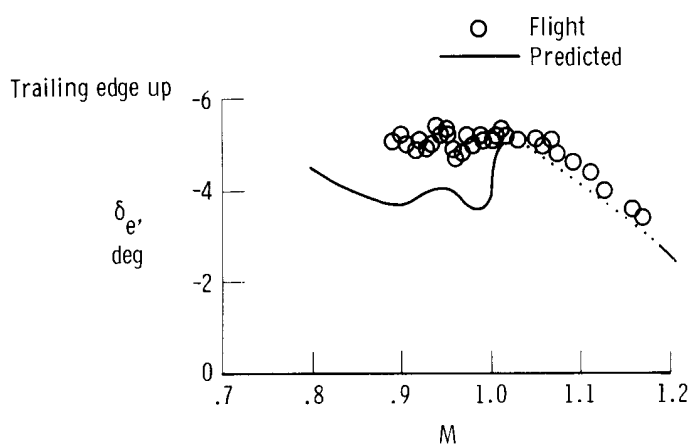

Figure 11. Transonic trim characteristics and comparison with predictions. h_p = 13,700 m; center of gravity = 22 percent $\bar{c}$.

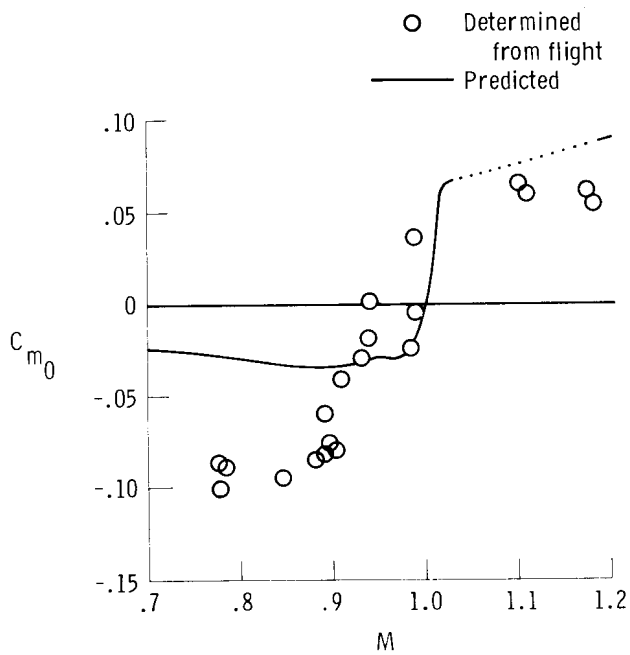

Figure 12. Zero lift pitching moment and comparison with predictions.

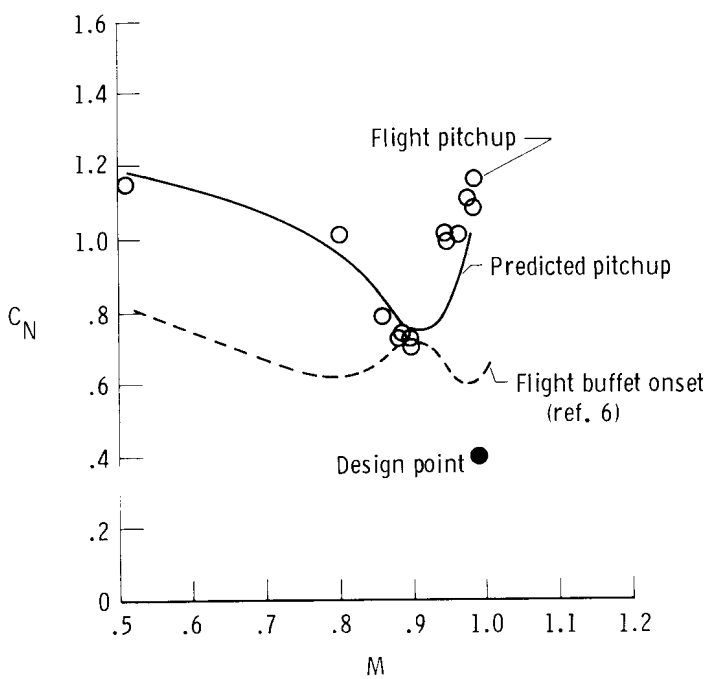

Figure 13. Longitudinal maneuvering characteristics from flight data and comparison with predicted pitchup.

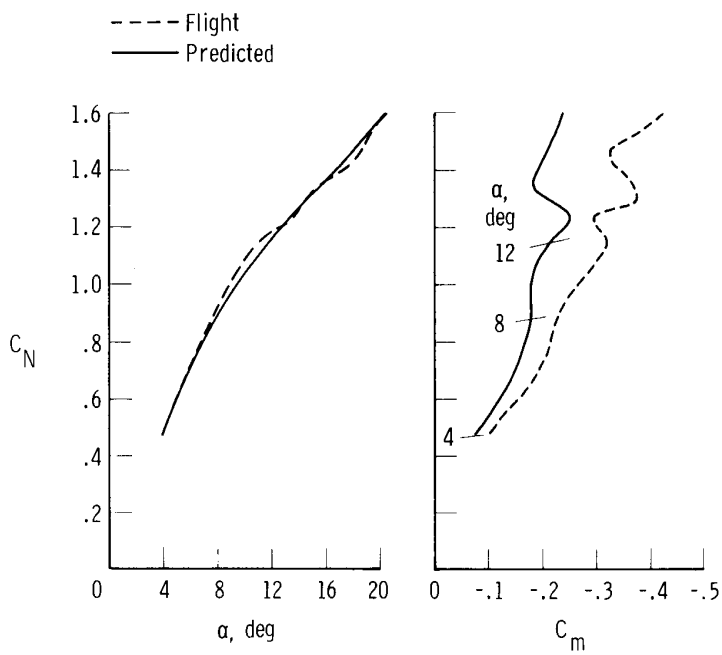

Figure 14. Longitudinal static characteristics from flight data and comparison with predictions. $M = 0.95$; $\delta_e = -2.5°$; center of gravity at 25 percent $\bar{c}$.

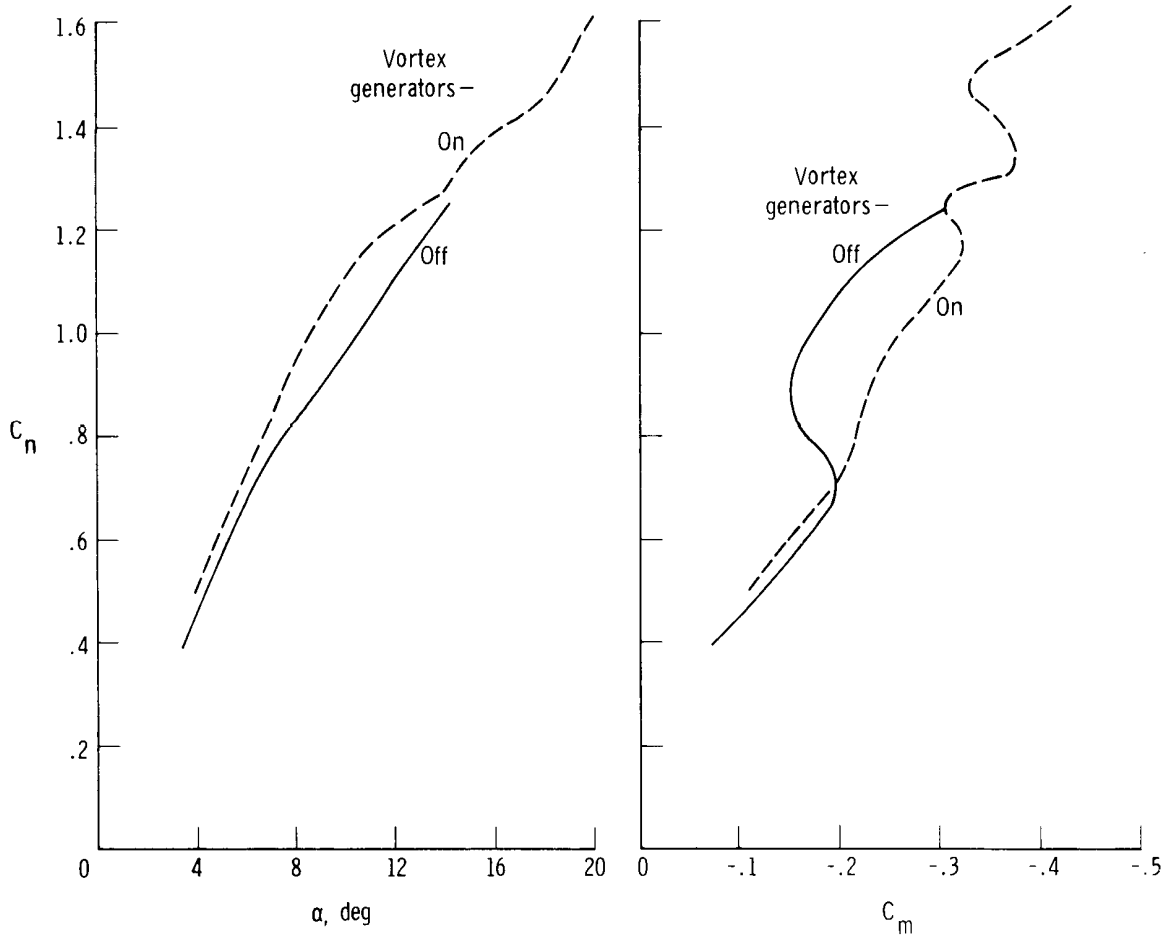

Figure 15. Effect of vortex generators on longitudinal static stability at Mach 0.95.

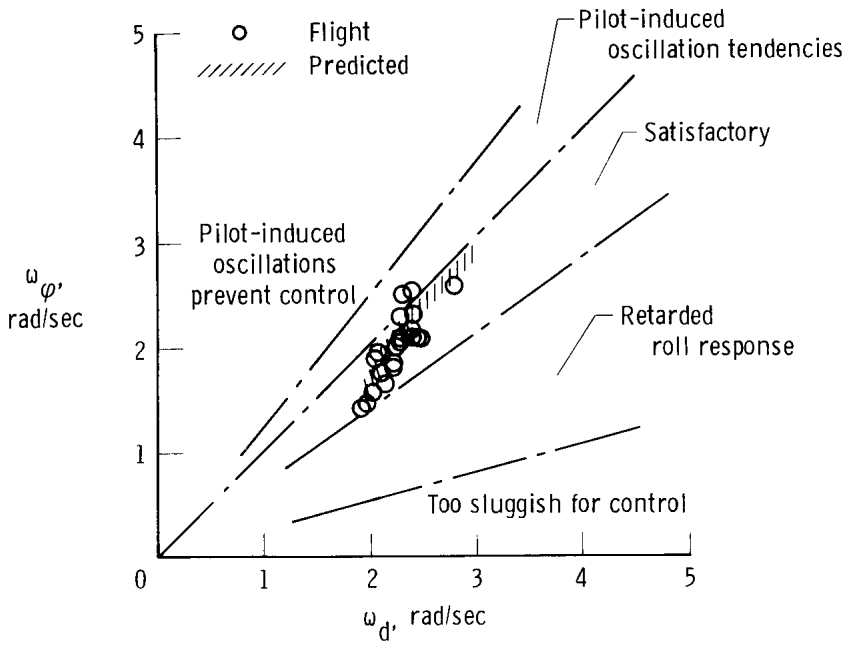

Figure 16. Comparison of flight and predicted lateral-directional coupling with the criteria of reference 16. M = 0.80 to 1.00.

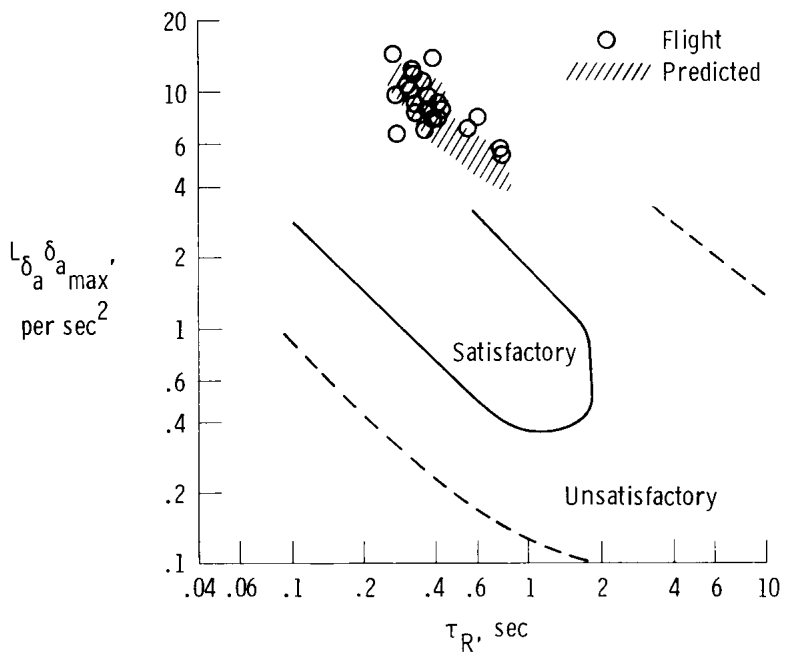

Figure 17. Comparison of flight and predicted roll control power with the criteria of reference 17. M = 0.80 to 1.00.

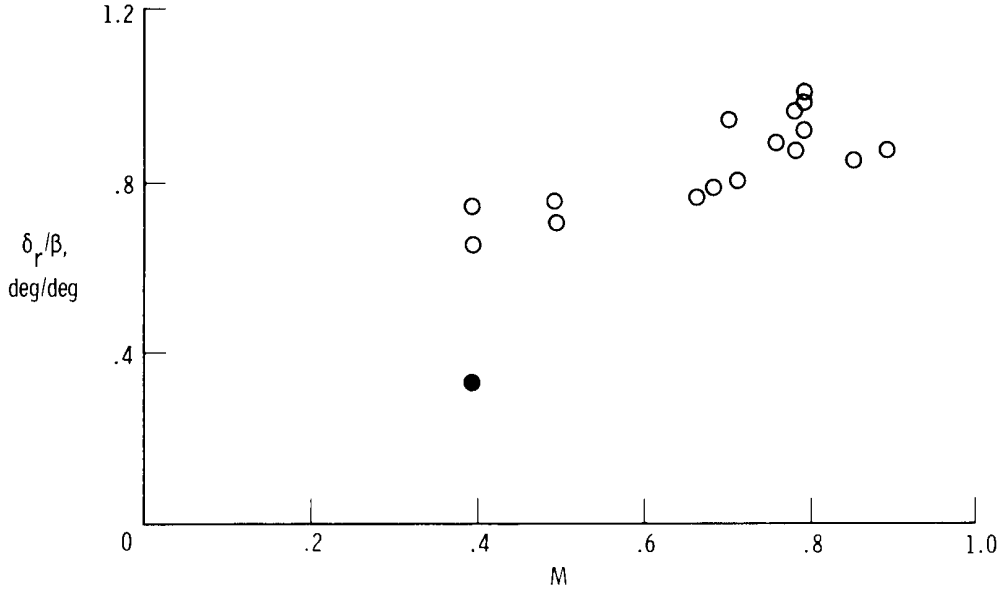

(a) Apparent directional stability.

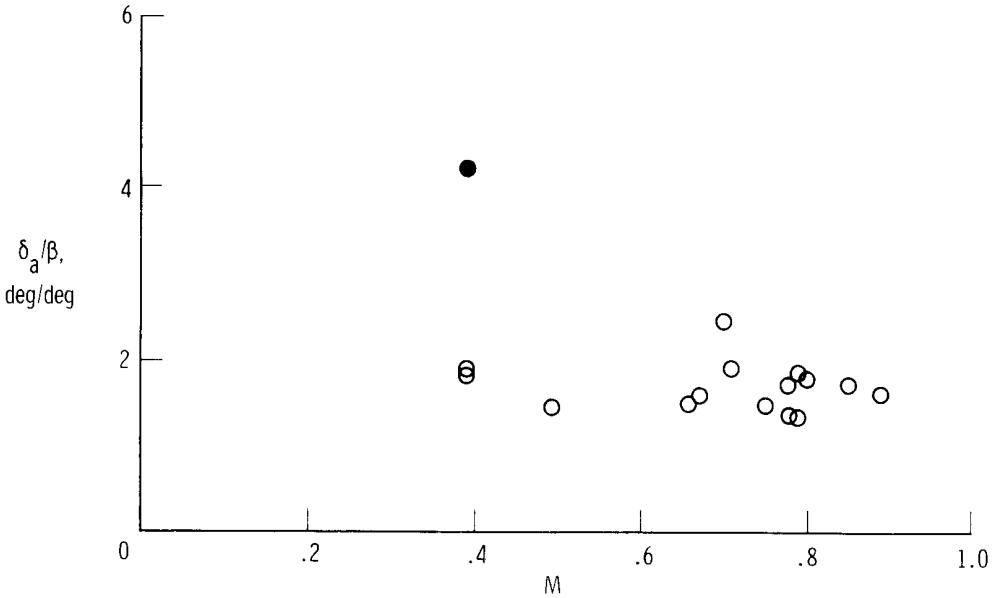

(b) Apparent effective dihedral.

Figure 18. Static directional stability characteristics. Data not corrected for center of gravity position; solid symbols denote flaps at 20°.

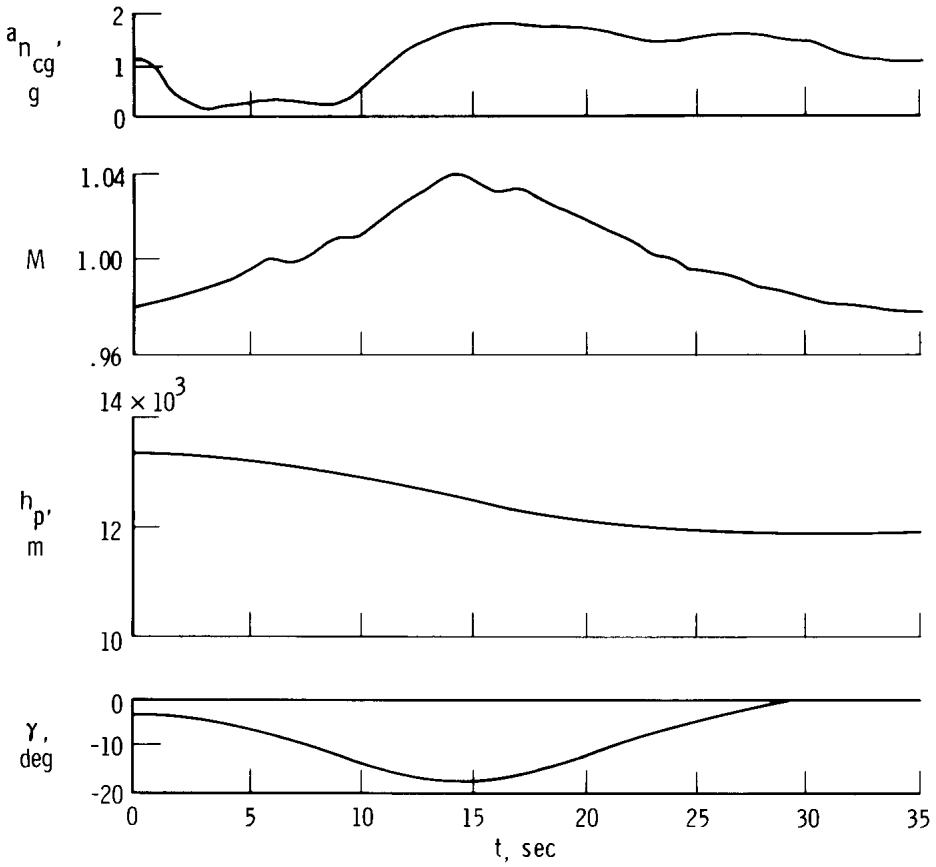

Figure 19. Simulated overspeed maneuver. Initiated at a bank angle of 45°.

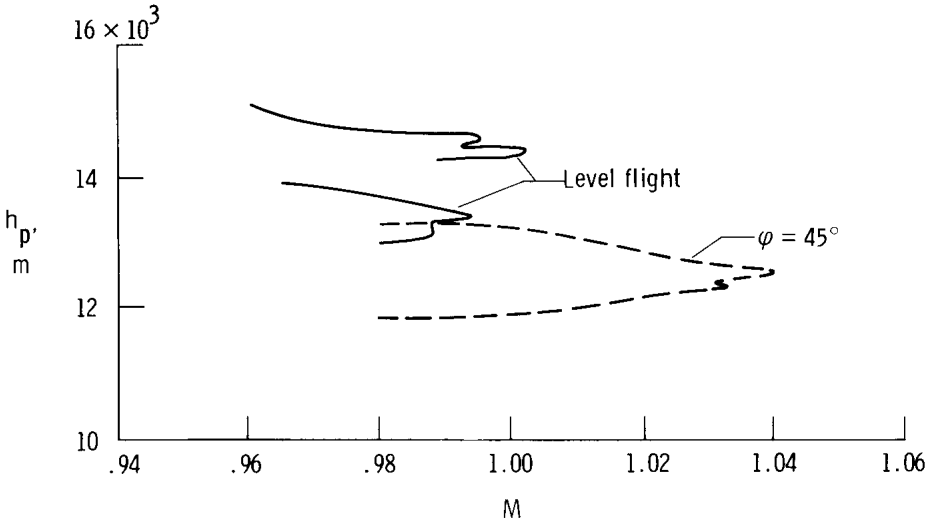

Figure 20. Summary of three simulated overspeed maneuvers.

1. Report No.	2. Government Accession No.	3. Recipient's Catalog No.
NASA TP-1167		

4. Title and Subtitle	5. Report Date
FLIGHT EVALUATION OF THE TRANSONIC STABILITY AND CONTROL CHARACTERISTICS OF AN AIRPLANE INCORPORATING A SUPERCRITICAL WING	February 1978
	6. Performing Organization Code
7. Author(s)	8. Performing Organization Report No.
Neil W. Matheny and Donald H. Gatlin	H-916
	10. Work Unit No.
9. Performing Organization Name and Address	505-06-31
Dryden Flight Research Center P. O. Box 273 Edwards, California 93523	11. Contract or Grant No.
	13. Type of Report and Period Covered
12. Sponsoring Agency Name and Address	Technical Paper
National Aeronautics and Space Administration Washington, D.C. 20546	14. Sponsoring Agency Code

15. Supplementary Notes

16. Abstract

A TF-8A airplane was equipped with a transport-type supercritical wing and fuselage fairings to evaluate predicted performance improvements for cruise at transonic speeds. A comparison of aerodynamic derivatives extracted from flight and wind tunnel data showed that static longitudinal stability, C_{m_α}; effective dihedral, C_{l_β}; and aileron effectiveness, $C_{l_{\delta_a}}$, were higher than predicted. The static directional stability derivative, C_{n_β}, was lower than predicted.

The airplane's handling qualities were acceptable with the stability augmentation system on. The unaugmented airplane exhibited some adverse lateral-directional characteristics that involved low Dutch roll damping and low roll control power at high angles of attack and roll control power that was greater than satisfactory for transport aircraft at cruise conditions. Longitudinally, the aircraft exhibited a mild pitchup tendency. Leading edge vortex generators delayed the onset of flow separation, moving the pitchup point to a higher lift coefficient and reducing its severity. The pitchup tendency, both with and without the vortex generators, was adequately masked by the stability augmentation system. No adverse handling qualities were observed during recovery from simulated upset and overspeed maneuvers from cruise conditions using normal piloting techniques.

17. Key Words (Suggested by Author(s))	18. Distribution Statement
Handling qualities Parameter estimation Stability and control Supercritical wing Transonic aerodynamics	Unclassified - Unlimited Category: 08

19. Security Classif. (of this report)	20. Security Classif. (of this page)	21. No. of Pages	22. Price*
Unclassified	Unclassified	62	$4.25

For sale by the National Technical Information Service, Springfield, Virginia 22161

NASA-Langley, 1978